$^{16}O + ^{48}Ca$ reaction at 56 MeV. I. Transitions to resolved levels

D. G. Kovar, W. Henning, B. Zeidman, Y. Eisen,* J. R. Erskine,
H. T. Fortune,† T. R. Ophel,‡ P. Sperr,§ and S. E. Vigdor**

(Received 23 August 1977)

All direct reaction channels of significant strength ($\sigma \geq 50$ μb) in the $^{16}O + ^{48}Ca$ reaction at $E_{lab}(^{16}O) = 56$ MeV were measured using a ΔE-E time-of-flight telescope system. Excitation spectra with energy resolutions ≈200 keV full width at half maximum were obtained for outgoing ions $^{11,12,13}B$, $^{12,13,14,15}C$, $^{14,15,16,17}N$, and $^{16,17,18,19}O$. Angular distributions were obtained for the strongest transitions observed in inelastic scattering, the single-nucleon transfer reactions (^{16}O, ^{15}N) and (^{16}O,^{17}O), the two-nucleon transfer reactions (^{16}O,^{14}C), (^{16}O,^{14}N), and (^{16}O,^{18}O), the three-nucleon transfer reactions (^{16}O,^{13}C), and the "exotic" transfers (^{16}O,^{16}N) and (^{16}O,^{15}C). Comparison of distorted-wave Born-approximation calculations for inelastic scattering, and for one- and two-nucleon transfer reactions to experiment suggest that reaction processes more complex than the one-step process are quite important in a majority of the transitions studied.

[NUCLEAR REACTIONS $^{48}Ca(^{16}O,^{16}O)$, $(^{16}O,^{16}O')$, $(^{16}O,^{17,18}O)$, $(^{16}O,^{14,15,16}N)$, $(^{16}O,^{13,14,15}C)$; measured $\sigma(\theta)$; $\theta = 4°$–$60°$, $\Delta\theta = 1$–$3°$, $^{48}Ca(^{16},^{19}O)$, $(^{16}O,^{17}N)$, $(^{16}O,^{12}C)$, $(^{16}O,^{11\text{-}13}B)$; measured σ. $E_{lab} = 56$ MeV, resolution 250 keV, enriched targets. Optical-model parameters deduced, DWBA calculations compared with data for $(^{16}O,^{16}O)$, $(^{16}O,^{17,18}O)$ $(^{16}O,^{14,15}N)$, and $(^{16}O,^{13,14}C)$.]

1. INTRODUCTION

Experimental studies of inelastic scattering and transfer reactions induced by heavy ions have generally fallen into one of two classes of measurements. On one hand, there have been measurements of inelastic and transfer reactions leading to resolved levels in the residual nuclei. These investigations have generally been limited to one or a few selected reaction channels. The attempts to understand the selectivity and angular distributions of these transitions have been carried out in the framework of a microscopic reaction theory, using distorted-wave Born approximation (DWBA) or coupled-channel Born approximation (CCBA) formalisms.[1] On the other hand, there have been investigations which have focused on the measurements of the summed "direct" reaction strength as function of mass transfer, angle, and excitation energy (Q value). These investigations have mainly established the systematics of the macroscopic cross section features. The attempts to understand these systematics have been carried out in the framework of classical or semiclassical models.[2] In addition, extensive studies have been made of the fusion cross sections in heavy-ion induced reactions.[3] Attempts to understand the energy and projectile dependence of the fusion process have been presented using classical and semiclassical models.[4,5] Despite all these studies, however, no complete set of measurements have been performed on a specific system so as to provide an overall picture of the distribution of the total reaction cross section (direct plus fusion cross section) or to relate the gross features of the direct reactions to specific characteristics of transitions leading to individual nuclear levels.

We report results of a study of the total reaction cross section of the $^{16}O + ^{48}Ca$ reaction at $E_L = 56$ MeV. Inelastic and transfer reaction channels as well as the fusion reaction were investigated. The inelastic and transfer reactions were observed with sufficient energy resolution to resolve individual levels and obtain angular distributions for transitions leading to many states of known spin and parity. In addition, direct reactions were measured over an excitation range sufficient to allow extraction of the total cross sections for each system of outgoing nuclei. The fusion or compound-formation cross sections were measured by detection of the recoiling heavy fragments at forward angles.

Taken together our measurements establish the detailed distribution of strength as well as the total reaction cross section. The results will be presented in two parts. In the present paper we present the results for inelastic and transfer reactions populating resolved nuclear levels.

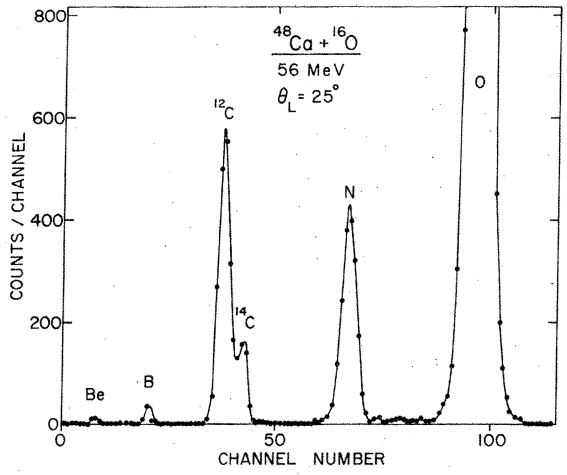

FIG. 1. A Z^2m spectrum obtained from ΔE^*E multiplication.

While emphasis is placed on the presentation of the systematic features observed in the experimental data, comparisons of DWBA calculations with the data also will be discussed in some detail.

II. EXPERIMENTAL TECHNIQUES AND DETAILS

Outgoing ions from boron to neon were detected and identified using a ΔE-E time-of-flight (TOF) telescope system previously described.[6] The telescope consisted of a ΔE silicon surface barrier detector (~17 μm) separated by ~25 cm from a thicker E silicon surface barrier detector (~200 μm). Analog electronic circuits generate an mZ^2 spectrum (Fig. 1) from ΔE and E signals and a mass spectrum (Fig. 2) from the time-of-flight t between the ΔE and E detectors by the relationship $t^2E \approx m$. Under normal conditions the system operated with intrinsic time resolutions of ~75–95 ps, energy resolutions of ~200–300 keV (FWHM), and an average energy range of ~20–30 MeV. As can be seen in Figs. 1 and 2 sufficient particle resolution is obtained to identify the detected ions unambiguously.

Beams of ^{16}O at 56 MeV incident energy from the Argonne FN tandem Van de Graaff accelerator were used to bombard isotopically enriched ^{48}Ca (~96.8%) targets of ~200 $\mu g/cm^2$ on carbon backings (~20 $\mu g/cm^2$). Absolute cross sections were obtained by normalizing the elastic scattering at forward angles to Rutherford scattering. Because of multiple scattering in the ΔE detector,

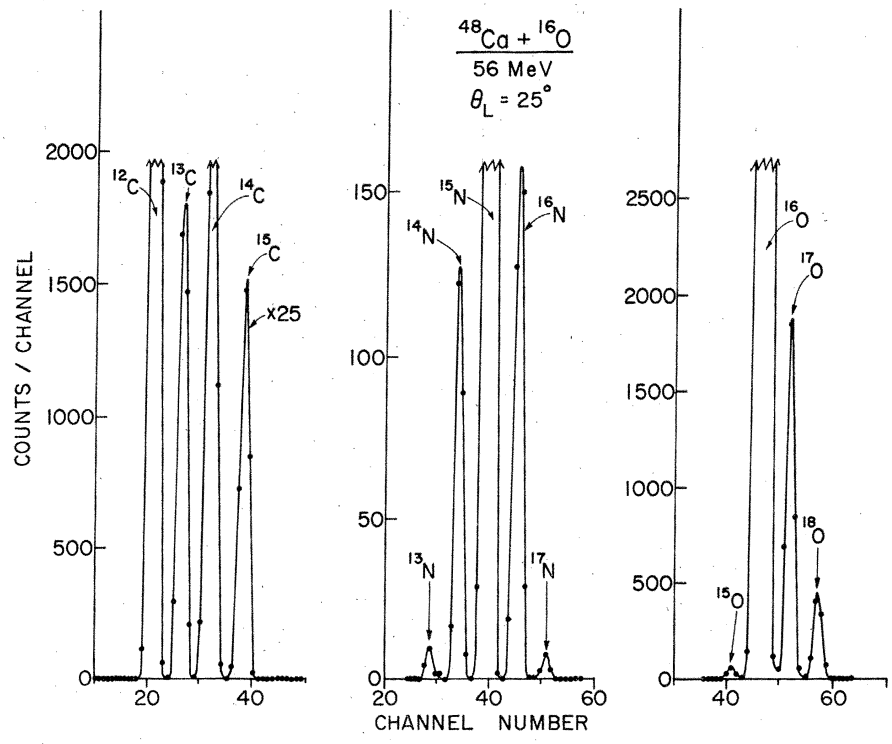

FIG. 2. Mass spectra obtained from the t^2*E multiplication.

scattering loss corrections which are dependent on both the charge and the energy of the detected particle had to be applied. The multiple-scattering losses of elastically scattered ^{16}O as a function of energy were measured for the telescope geometry used, by comparing the yield observed in the ΔE-E TOF system to that observed in a single E detector. These results were compared with multiple-scattering losses predicted using the theory of Williams.[7] While the energy dependence was well reproduced, the predicted magnitude had rather large uncertainties due to sensitivity to the beam spot properties and to the exact geometry. The measured ^{16}O losses were used to normalize the multiple-scattering calculations. The normalized calculations were then used to generate the correction factors for all isotopes measured. Since the cross sections were obtained by normalizing the elastic scattering at forward angles to Rutherford, the relative multiple-scattering corrections at backward angles amounted to as much as ~30–40% for oxygen isotopes, but only ~20% for carbon and boron isotopes. The absolute cross sections are believed to be accurate to better than 10% and the relative cross sections to better than 5% for all isotopes.

In specific cases where the energy resolution was an important factor in determining which levels were populated and where closely spaced levels needed to be resolved for the extraction of angular distributions of interest, measurements were made with the Argonne split-pole magnetic spectograph. The outgoing ions were detected in a ionization-chamber focal-plane detector system.[8] This system allowed unambiguous particle identification using the parameters ΔE, E, and $B\rho$. In order to obtain cross sections from yields, charge state corrections were applied; the corrections were determined by measuring the charge state distribution as a function of energy for the isotopes of interest. Again the absolute cross sections were established by using the elastic scattering at forward angles. In all cases the cross sections extracted from the spectograph measurements were found to agree within errors with the cross sections obtained in the TOF measurements.

III. GENERAL COMMENTS ON EXPERIMENTAL RESULTS

The reaction channels for which excitation spectra were obtained are indicated in Fig. 3. All boron, carbon, nitrogen, and oxygen isotopes with total reaction cross sections greater than ~100 μb were measured. Fluorine and neon isotopes were detected; however, contaminants on the target together with the small cross section ($\lesssim$50 μb) for these channels prevented extraction of meaningful

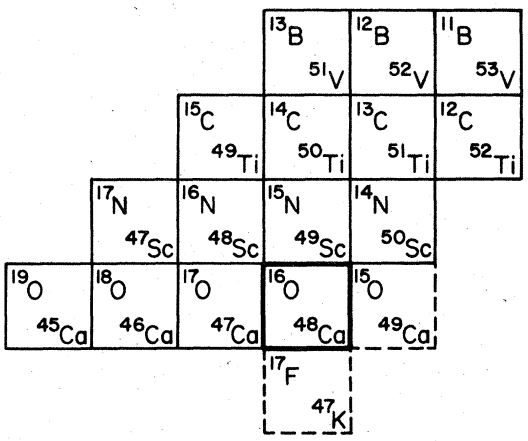

FIG. 3. Schematic diagram indicating those channels for which excitation spectra were obtained. The dashed blocks indicate channels for which only upper limits on the cross section were obtained.

spectra. For the lighter outgoing ions Be and Li the total cross sections were much weaker than for the B isotopes and not recorded. In order to give some indication of the relative strengths of inelastic and transfer channels, the angle-integrated reaction cross sections for transitions in each reaction channel measured are listed in Table I. In most cases the listed transitions correspond to transfers to the ground state or levels at low excitation with the outgoing particle in its ground state. The table clearly indicates that the cross sections decrease rapidly with increasing number of nucleons transferred. This appears to be the case regardless of whether the nucleons can be transferred as a "cluster" [e.g., ($^{16}O, ^{13}C$)] or not [e.g., ($^{16}O, ^{15}C$)]. The very small transfers observed for the proton pickup reactions such as ($^{16}O, ^{17}F$) and the neutron stripping reactions such as ($^{16}O, ^{15}O$) are a result of the severe kinematic mismatch of these reactions.

In Figs. 4–7 energy spectra obtained with the ΔE-E-TOF system for the outgoing B, C, N, and O isotopes are shown. In most cases the spectra are those measured at $\theta_{lab} = 25°$. In cases where the cross sections were too small to obtain a meaningful spectrum at a single angle, the spectra shown were obtained by summing kinematically corrected spectra measured at several angles. The energy resolution of ~250 keV full width at half maximum (FWHM) was sufficient to separate and identify the levels labeled in Figs. 4–7; angular distributions for most of these will be shown later.

There are several general features in the spectra which should be noted. In all reactions the strongly populated levels in the residual nuclei

TABLE I. Cross sections observed for representative low-lying levels populated in the reaction channels measured.

Nucleons transfered	Reaction	ΔN	State populated	Q value (MeV)	σ (mb)
0	$(^{16}O, ^{16}O')$	0	$^{48}Ca(2^+)$	−3.83	6.04
			$^{48}Ca(3^-)$	−4.51	5.67
1	$(^{16}O, ^{15}N)$	$-1p$	$^{49}Sc(\frac{7}{2}^-)_{g.s.}$	−2.50	10.29
	$(^{16}O, ^{17}O)$	$+1n$	$^{47}Ca(\frac{7}{2}^-)_{g.s.}$	−5.80	10.88
	$(^{16}O, ^{15}O)$	$-1n$	$^{49}Ca(\frac{3}{2}^-)_{g.s.}$	−10.52	≤0.03
	$(^{16}O, ^{17}F)$	$+1p$	$^{47}K(\frac{3}{2}^+)_{g.s.}$	−14.66	≤0.03
2	$(^{16}O, ^{14}C)$	$-2p$	$^{50}Ti(0^+)_{g.s.}$	−0.54	0.370
			$^{50}Ti(2^+)$	−2.09	0.480
	$(^{16}O, ^{14}N)$	$-1p1n$	$^{50}Sc(5^+)_{g.s.}$	−6.85	0.147
	$(^{16}O, ^{18}O)$	$+2n$	$^{46}Ca(0^+)_{g.s.}$	−5.03	0.190
	$(^{16}O, ^{16}N)$	$+1p-1n$	$^{48}Sc(6^+, 5^+, 4^+)_{g.s.}$ [a]	−10.13	0.168
3	$(^{16}O, ^{13}B)$	$-3p$	$^{51}V(\frac{7}{2}^-)_{g.s.}$	−13.32	≤0.007
	$(^{16}O, ^{13}C)$	$-2p1n$	$^{51}Ti(\frac{3}{2}^-)_{g.s.}$	−2.34	0.042
	$(^{16}O, ^{19}O)$	$+3n$	$^{45}Ca(\frac{7}{2}^-)_{g.s.}$	−11.48	≤0.003
	$(^{16}O, ^{15}C)$	$-2p+1n$	$^{49}Ti(\frac{7}{2}^-)_{g.s.}$	−10.27	0.003
			$^{49}Ti(\frac{5}{2}^-, \frac{7}{2}^-)$	−12.53	0.019
4	$(^{16}O, ^{12}C)$	$-2p-2n$	$^{52}Ti(0^+)_{g.s.}$	+0.51	≤0.002
			$^{52}Ti(2^+)$	−0.54	≤0.012
	$(^{16}O, ^{12}B)$	$-3p-1n$	$^{52}V(1^+-5^+)_{g.s.}$ [a]	−10.89	<0.002
5	$(^{16}O, ^{11}B)$	$-3p-2n$	$^{53}V(\frac{3}{2}^-, \frac{5}{2}^-, \frac{7}{2}^-)_{g.s.}$ [a]	−5.44	<0.004

[a] Unresolved ground-state groups.

are the same as those populated in the analogous light-ion reactions after kinematic matching conditions are taken into account. Moreover, in all reactions there is evidence that the excited states of the light outgoing particles are populated in many cases as strongly as their ground states. Finally, reactions involving the transfer of two or more protons exhibit energy spectra of roughly Gaussian shape with centroids located at a relatively large excitation energy. The energy resolution does not make it possible to determine whether these are smooth continuum distributions or rather the result of populating many closely spaced discrete levels.

IV. ELASTIC SCATTERING

The elastic scattering of ^{16}O ions on ^{48}Ca at $E_L(^{16}O) = 56$ MeV was measured with both the ΔE-E-TOF and magnetic spectrograph detection systems. The elastic scattering angular distribution $\sigma_{el}/\sigma_{Ruth}$ is shown in Fig. 8 together with an optical-model fit to the data. As mentioned previously the elastic scattering at forward angles was set equal to the Rutherford cross section in order to establish the absolute cross section. The uncertainty in this normalization to Rutherford arises from the uncertainty in determining angles ($\lesssim 0.1°$) and from the uncertainty in fitting to Rutherford. In addition there is ~3% admixture of ^{40}Ca in our target whose elastic yield at forward angles is not resolvable from that due to ^{48}Ca. Since $^{16}O + ^{40}Ca$ elastic scattering was measured, its contribution was subtracted from $^{16}O + ^{48}Ca$ elastic scattering. The overall uncertainty in the absolute cross section is believed to be $\lesssim 5\%$.

The optical model search codes GENOA [9] and

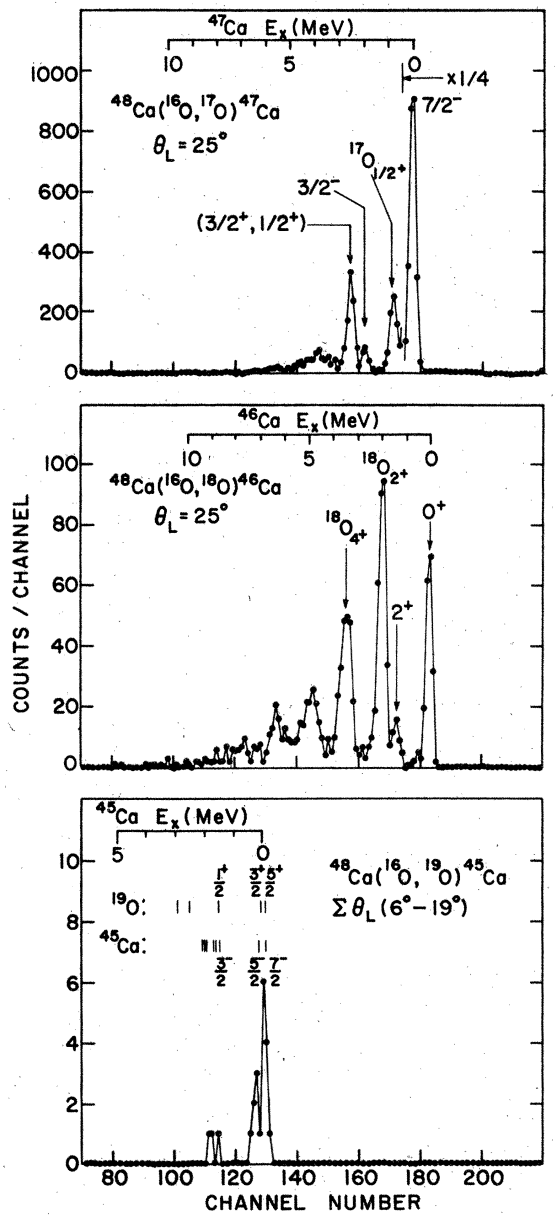

FIG. 4. Excitation spectra obtained for the oxygen isotopes at $\theta_{lab} = 25°$. The ^{19}O spectrum was obtained by summing kinematically corrected spectra measured at angles $6° \leq \theta_{lab} \leq 19°$.

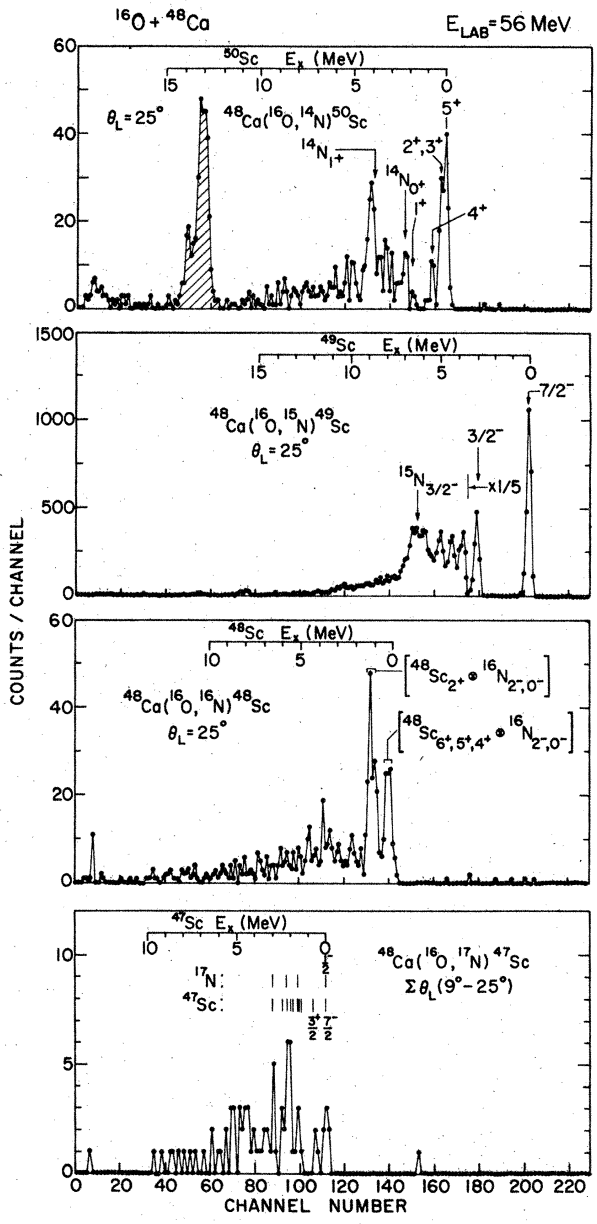

FIG. 5. Excitation spectra obtained for the nitrogen isotopes at $\theta_{lab} = 25°$. The ^{17}N spectrum was obtained by summing kinematically corrected spectra measured in the angular range $9° \leq \theta_{lab} \leq 25°$. The shaded peak in the ^{14}N spectrum arises from a reaction initiated on the carbon backing of the target.

ABACUS [10] were used to fit the elastic scattering angular distribution. The potential used was of the form

$$V(r) = V^C(r) - Vf(r) - iWg(r),$$

where

$$V^C(r) = \begin{cases} Z_1 Z_2 e^2/r, & r > R_C \\ Z_1 Z_2 e^2/2R_C(3 - r^2/R_C^2), & r < R_C \end{cases}$$

$$R_C = r_{0C}(A_1^{1/3} + A_2^{1/3}),$$

$$f(r) = \left[1 + \exp\left(\frac{r - R_r}{a_r}\right)\right]^{-1}, \quad R_r = r_{0r}(A_1^{1/3} + A_2^{1/3}),$$

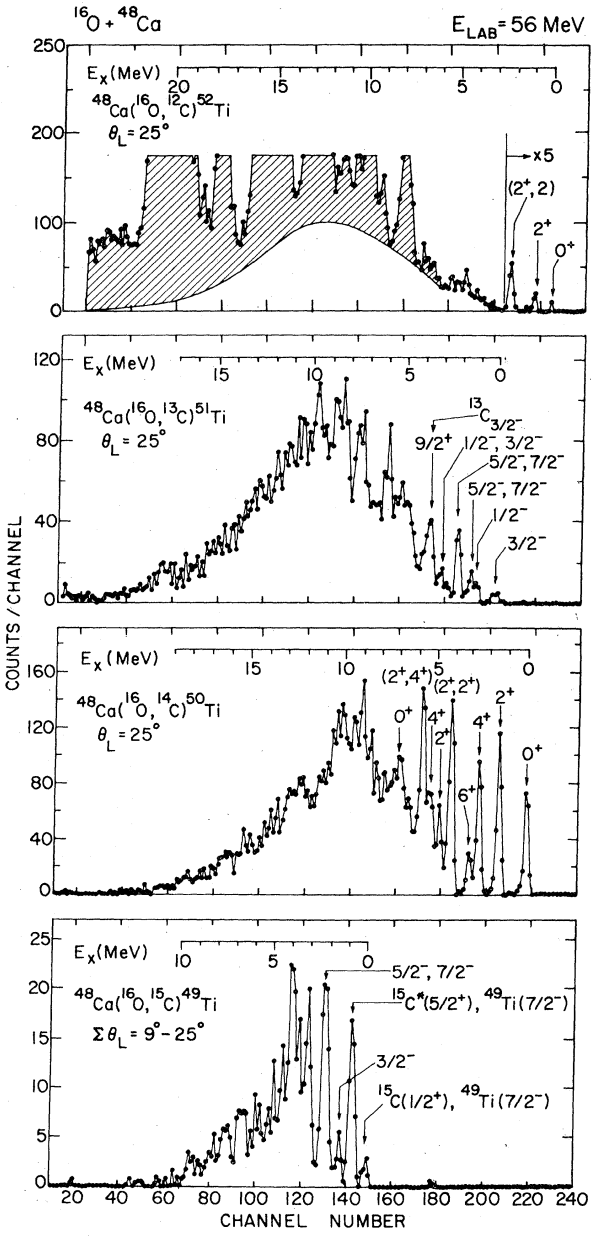

FIG. 6. Excitation spectra obtained for the carbon isotopes at θ_{lab}=25°. The ^{15}C spectrum by summing kinematically corrected spectra measured at angles $9° \leq \theta_{lab} \leq 25°$. The shaded regions in the ^{12}C spectrum are attributed to reactions initiated on the carbon backing or on an ^{16}O contaminant in the target.

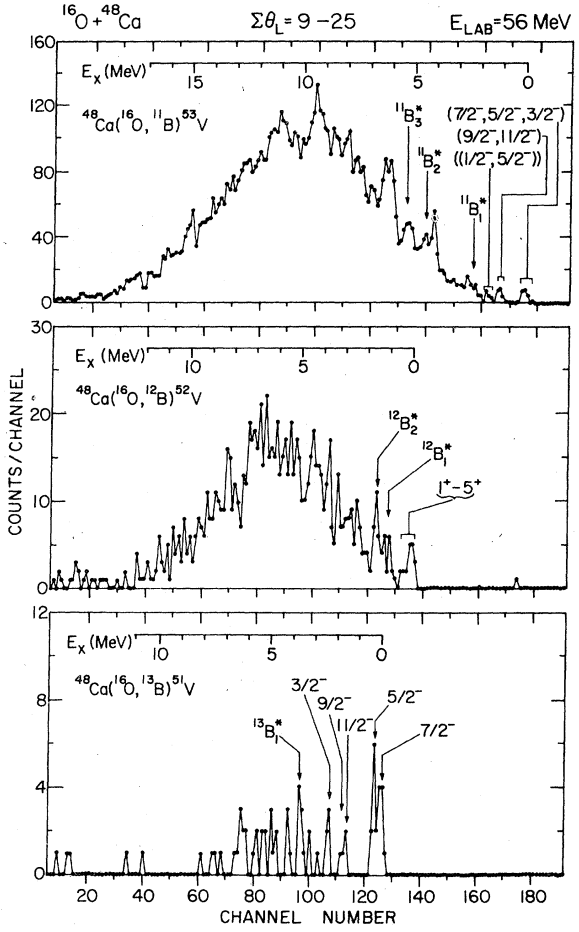

FIG. 7. Excitation spectra obtained for the boron isotopes obtained by summing kinematically corrected spectra measured at angles $9° \leq \theta_{lab} \leq 25°$.

$$g(r) = \left[1 + \exp\left(\frac{r - R_i}{a_i}\right)\right]^{-1}, \quad R_i = r_{0i}(A_1^{1/3} + A_2^{1/3}).$$

In these expressions A_1, Z_1 and A_2, Z_2 are the mass and charge of the projectile and target nucleus, respectively. The curve shown in Fig. 8 was generated by the parameters listed in Table II. This parameter set is one of several obtained in a study[11] of elastic scattering of ^{16}O + ^{48}Ca at 56 MeV where it was shown that when six parameters (V, r_{0r}, a_r, W, r_{0i}, and a_i) were allowed to vary, essentially equivalent fits could be obtained with parameter sets which differed considerably in geometries and well depths. In addition it was shown that when these different potentials are used in DWBA calculations for single-nucleon transfers, essentially identical angular distributions are predicted. Based on these results no extensive discussion of the effect of optical-potential ambiguities on DWBA transfer calculations will be presented here. In the DWBA calculations which appear later, the optical-model parameter set listed in Table II (parameter set A3 in Ref. 11) will be used in both the entrance and exit channel.

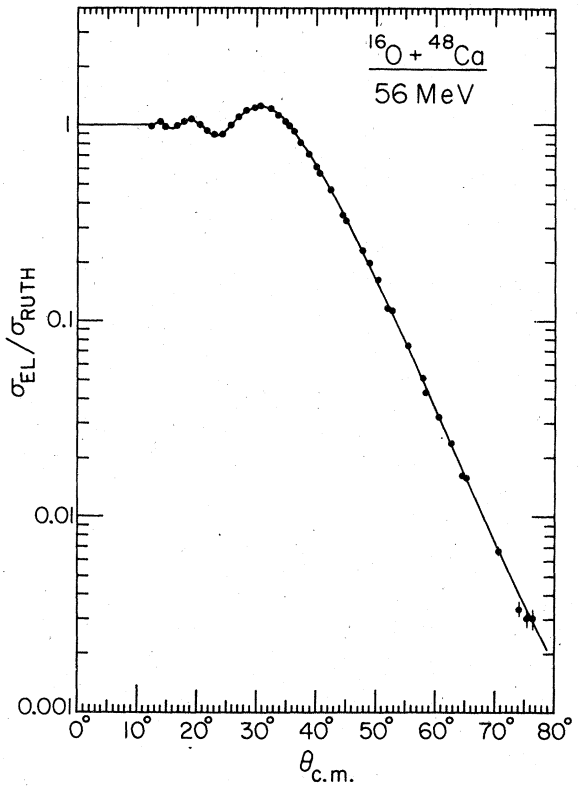

Fig. 8. Elastic scattering angular distribution $d\sigma_{el}/d\sigma_{Ruth}$) measured for $^{16}O + ^{48}Ca$ at $E_{lab} = 56$ MeV. The solid curve is the optical-model fit using the parameters in Table II.

TABLE II. Optical-model parameters obtained in fit to elastic scattering and used in DWBA calculations.

V (MeV)	r_{0r} (fm)	a_r (fm)	W (MeV)	r_{0i} (fm)	a_i (fm)	r_{0C} (fm)
100.1	1.200	0.500	24.0	1.207	0.482	1.200

V. INELASTIC SCATTERING

A. Results

To study the inelastic scattering, measurements were made both with the TOF telescope and the magnetic spectrograph. The inelastic excitation spectrum obtained at $\theta_{lab} = 32°$ in the spectrograph is shown in Fig. 9. The states most strongly populated are the lowest-lying 2^+ and 3^- levels in ^{48}Ca at $E_x = 3.832$ and 4.505 MeV, respectively. At an excitation energy of ≈ 6.0 MeV the rather broad peak observed may correspond to the inelastic excitation of the $^{16}O(3^-)$ state at $E_x = 6.13$ MeV. However, no angular distribution was extracted because of difficulties in unambiguously identifying the strength over a large angular range. The elastic scattering from the ^{40}Ca contaminant can clearly be seen in Fig. 9. Over a narrow angular region the inelastic excitation of the first excited

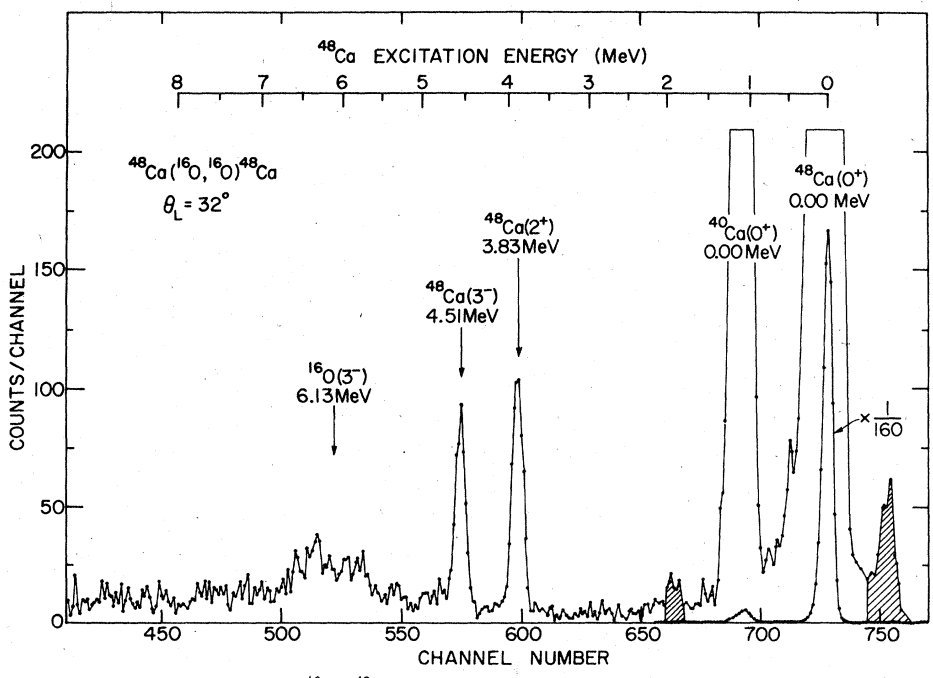

FIG. 9. Inelastic excitation spectrum for $^{16}O + ^{48}Ca$ obtained with the magnetic spectrograph. Shaded peaks arise from contaminants.

3^- state in ^{40}Ca at $E_x = 3.73$ MeV falls into the same region of the energy spectrum as the ^{48}Ca states of interest and hence could potentially disturb their angular distributions. However, from the strength of the contaminant ^{40}Ca elastic scattering and the ^{40}Ca(3^-) angular distribution which will be reported elsewhere,[12] we estimate that the contributions to our ^{48}Ca states are <3% in the region of overlap.

B. DWBA Analysis

Measured angular distributions associated with the ^{48}Ca(2^+) and ^{48}Ca(3^-) levels are shown in Fig. 10 together with the predicted angular distributions as calculated by the heavy-ion code PTOLEMY. While the details of this reaction code are discussed elsewhere,[13] it is noteworthy to remark here that PTOLEMY explicitly calculated the Coulomb-excitation process to high angular momentum (i.e., $l \geq 500$) without resorting to semiclassical approximations. The form factors used in our calculations were those of the traditional macroscopic model[14] which is based on treating inelastic scattering as the excitation of a collective mode. In this model the form factor has a Coulomb and nuclear part and can be written as

$$F_L(r) = F_L^C(r) + F_L^N(r),$$

where

$$F_L^C(r) = \frac{4\pi Z_1 e [B(EL)]^{1/2}}{2L+1} \begin{cases} \dfrac{1}{r^{L+1}}, & \text{for } r > R_{C2} \\ \dfrac{r^L}{R_{C2}^{2L+1}}, & \text{for } r < R_{C2} \end{cases}$$

with

$$R_{C2} = r_{0C} A_2^{1/3}$$

and

$$F_L^N(r) = \left(\beta_L^N R_2 V \frac{df(r)}{dr} + i \beta_L^N R_{I2} W \frac{dg(r)}{dr} \right)$$

with

$$R_2 = r_{0r} A_2^{1/3} \text{ and } R_{I2} = r_{0i} A_2^{1/2} .$$

In these expressions $B(EL)$ is the electromagnetic reduced transition probability for Coulomb excitation of the target, and β_L^N is the mass deformation of multipolarity L.

The "charge deformation length" ($\delta_L^C \equiv \beta_L^C R_{C2}$) is related to the reduced transition probability $B(EL)$ via the expression,[15]

$$B(EL;\uparrow) = (3/4\pi)^2 e^2 Z_2^2 (\beta_L^C)^2 R_{C2}^{2L},$$

where $R_{C2} = 1.20 A_2^{1/3}$ was used in the present calculations. Measurements of (e, e') (Ref. 16) and $(p, p'\gamma)$ (Ref. 17) have established the reduced electromagnetic transition probabilities for the 2^+ and 3^- states. Using the values for the charge deformation lengths deduced from the (e, e') studies of Eisenstein *et al.*,[16] and varying the nuclear deformation lengths ($\delta_L^N \equiv \beta_L^N R_2$) to fit the observed angular distributions the best results obtained are those shown in Fig. 10, where the primary criterion in the fit was reproduction of the observed magnitude.

From Fig. 10 we see that while there are some noticeable discrepancies, the overall shapes of the angular distributions are fairly well reproduced. Among the discrepancies is the inability of the calculations to reproduce, (1) the location of the interference dip observed for the 2^+ excitation near 30°, (2) the behavior at the most forward angles for the 3^- excitation, and (3) the falloff of cross section at large angles for both excitations. Similar discrepancies have been observed in previous comparisons of DWBA with experiment and possible explanations have been proposed.[18-22] A discussion of these discrepancies (and those observed for other Ca isotopes) will be presented

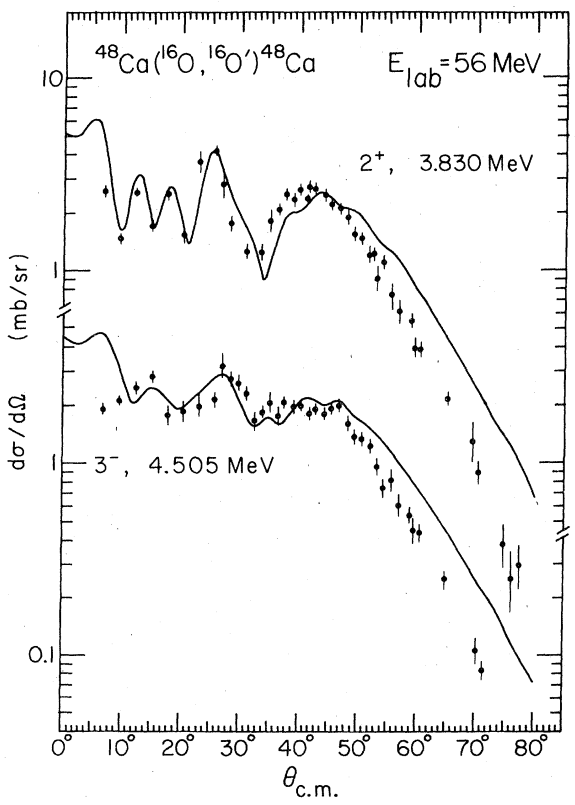

FIG. 10. Inelastic scattering angular distributions extracted for the ^{48}Ca(2^+) and ^{48}Ca(3^-) states. The solid curves are DWBA calculations discussed in the text.

TABLE III. Comparison of deformation lengths extracted in analyses of inelastic scattering to the $^{48}Ca(2^+)$ and $^{48}Ca(3^-)$ states.

E_x		(^{16}O, $^{16}O'$) present work				(e,e') [a,b]	$(p,p'\gamma)$ [b,c]	(p,p') [d]	(p,p') [e]	(d,d') [f]	(a,a') [g]
(MeV)	J^π	β_L^C	β_L^N	δ_L^C	δ_L^N	δ_L^C	δ_L^C	δ_L^N	δ_L^N	δ_L^N	δ_L^N
3.832	2^+	0.103	0.161	0.451	0.70	0.451 ± 0.169	0.468 ± 0.305	0.70	1.00	0.61	0.71
4.505	3^-	0.204	0.170	0.889	0.741	0.889 ± 0.344	$1.090 \pm {}^{0.846}_{0.597}$	0.810	1.15	0.65	0.76

[a] Reference 16.
[b] β_L^C obtained using the expression $\beta_L^C = 4\pi[B(EL;\uparrow)]^{1/2}/3Z_2e(R_C)^L$ and $R_C = 1.20\ A_2^{1/3}$.
[c] Reference 17.
[d] Reference 23.
[e] Reference 24.
[f] Reference 25.
[g] Reference 26.

in a forthcoming publication[12] and will not be pursued here.

The charge and nuclear (mass) deformation lengths used to generate the fits in Fig. 10 are listed in Table III where they are compared with those obtained from other studies.[16,17,23-26] The nuclear deformation needed to fit the 3^- angular distribution differs by only ≈20% from the charge deformation inferred from Coulomb excitation.[16] For the 2^+ state, however, the nuclear deformation implied by our results differs from the charge deformation extracted from Coulomb excitation[16] by almost 60%. From the table it can be noted that the nuclear deformation lengths obtained from our fits are consistent with those obtained from *p*, *d*, and α inelastic scattering reactions[23-26] which are almost exclusively sensitive to the nuclear deformations. While the results of the various measurements do suggest that the charge and mass deformations are different, it must be remembered that the macroscopic form factors used may not be appropriate for the 2^+ state. Moreover, coupled-channel calculations performed[27] indicate that ≈30% changes in the strength may be expected. Hence calculations in which microscopic form factors and coupled-channel effects are included should be performed before any definite conclusions regarding the mass deformations are drawn.

VI. SINGLE-NUCLEON TRANSFERS

A. Experimental Results

1. $^{48}Ca(^{16}O,^{15}N)^{49}Sc$

An energy spectrum obtained for the $^{48}Ca(^{16}O, ^{15}N)^{49}Sc$ reaction is shown in Fig. 5. Excited strongly are the two lowest-lying "single-proton" states; the $\frac{7}{2}^-$ ground state ($1f_{7/2}$) and the $\frac{3}{2}^-$ state ($2p_{3/2}$) at $E_x = 3.08$ MeV in ^{49}Sc. The angular distributions associated with these states, shown in Fig. 11, are characterized by pronounced strength near the grazing angle and oscillatory behavior of significant strength at forward angles. As has been discussed previously the structure at forward angles is related to the transferred angular momentum L and under certain conditions may be used to identify the J^π of the final state.[28,29]

Also shown in Fig. 11 are angular distributions for transfers to a group observed at $E_x = 2.3$ MeV and to a broad group at $E_x \cong 6.3$ MeV. At an excitation near 2.3 MeV in ^{49}Sc there are two known levels,[30,31] a $\frac{1}{2}^+$ state at 2.20 MeV and a $\frac{3}{2}^+$ state at 2.37 MeV. These states are weakly excited in $(^3He, d)$ and (α, t) reactions (i.e., $C^2S = 0.05$–0.10)[30-32] and are believed to be of predominantly two-particle–one-hole (2p-1h) character. In our TOF measurements the two states could not be resolved. In measurements with the magnetic spectrograph these levels were resolved as shown in Fig. 12, and their relative intensities were measured; however, the low yields prevented the extraction of unambiguous angular distributions. The angular distribution shown in Fig. 11 is that observed for the doublet. The broad level at $E_x = 6.3$ MeV is clearly evident in the spectra obtained at angles $\theta_{lab} > 25°$, where it becomes a dominant feature in the excitation spectrum. At more forward angles other strength in this excitation region prevented an unambiguous extraction of the yield for this level. The excitation energy and width observed are consistent with an identification of this level as the Doppler broadened $\frac{3}{2}^-$ state of ^{15}N at $E_x = 6.332$ MeV. Evidence for the observation of this excited state has previously been reported in studies of the (^{16}O, ^{15}N) reactions on Sr and Zr isotopes.[33] Other states identified in the higher resolution spectrum obtained with the spectrograph are labeled in Fig. 12. No angular distributions were extracted for these.

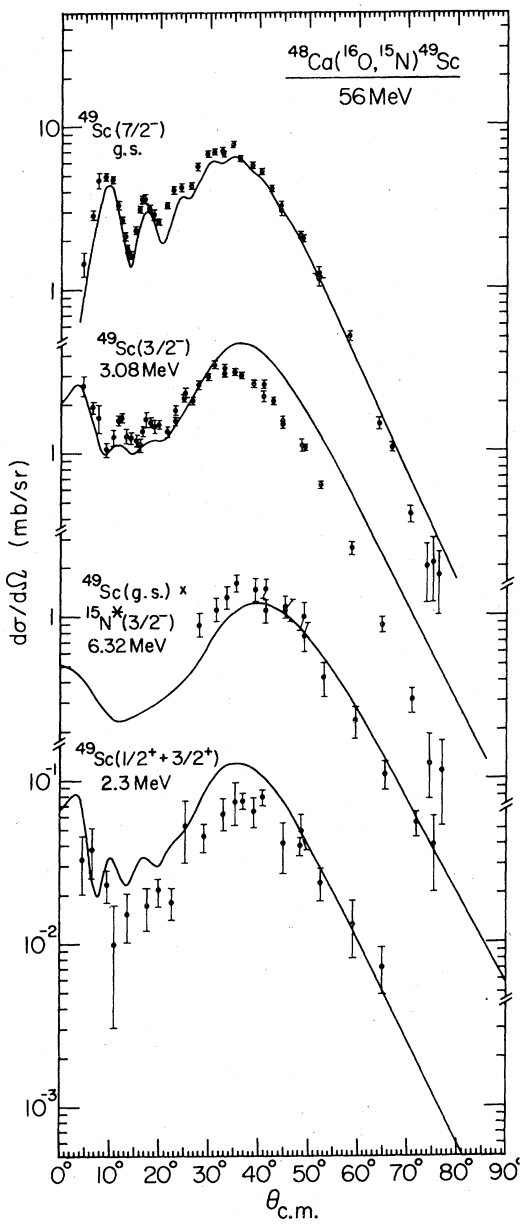

Fig. 11. Angular distributions obtained for the (^{16}O, ^{15}N) reaction. The solid curves are DWBA predictions using spectroscopic factors obtained in light-ion studies discussed in the text.

2. $^{48}Ca(^{16}O,^{17}O)^{47}Ca$

The energy spectrum obtained for ^{48}Ca(^{16}O, ^{17}O)-^{47}Ca at $\theta_{lab} = 25°$ is shown in Fig. 4. Four levels were identified and angular distributions extracted. The strongest transitions observed were to the well-known "single-neutron hole" states in ^{47}Ca; the $1f_{7/2}^{-1}$ ground state and the $1d_{3/2}^{-1}$ and $2s_{1/2}^{-1}$ states at $E_x = 2.580$ and 2.602 MeV, respectively. The energy resolution in our measurements did not permit separation of the two states near $E_x \approx 2.6$ MeV even with the spectrograph. Also observed were a level at $E_x = 0.89$ MeV, which was identified as the transfer to the ^{47}Ca ground state leaving the outgoing ^{17}O in its first excited state ($\frac{1}{2}^+$, 0.89 MeV), and a level at $E_x \approx 2.00$ MeV which was identified as the population of the $\frac{3}{2}^-$ one-particle–two-hole (1p-2h) state at $E_x = 2.016$ MeV in ^{47}Ca.

The angular distributions for these four transitions are shown in Fig. 13. The most notable feature is the qualitative difference between the shapes of the angular distributions for the transfers to single-hole states and for the transfers leaving ^{17}O in its excited state and that leading to the 1p-2h state. The pickup reactions leading to the single-hole states show angular distributions which are bell-shaped, centered near the grazing angle, with some strength at forward angles. The other two transfers show no pronounced strength near the grazing angle, but have nearly constant strength at forward angles. At larger angles but still forward of the grazing angle, the cross sections begin to decrease rapidly. The angular distributions for the (^{16}O, ^{17}O) transfers to the single-hole states do not show the pronounced oscillatory pattern noted in the (^{16}O, ^{15}N) reactions. This behavior is consistent with DWBA calculations which show that it is a result of the greater kinematic mismatch in the neutron pickup reaction.

3. $^{48}Ca(^{16}O,^{17}F)^{47}K$ and $^{48}Ca(^{16}O,^{15}O)^{49}Ca$

No energy spectra or angular distributions were obtained for the proton-pickup reaction (^{16}O, ^{17}F) or the neutron-stripping reaction (^{16}O, ^{15}O) because of low yields in these channels, and the presence of contaminants. Based on our data we estimate the angle-integrated cross sections for these reactions leading to the ground states of ^{47}K and ^{49}Ca to be $\lesssim 30$ μb.

B. DWBA analysis

The DWBA calculations were performed with the exact finite-range program PTOLEMY.[13] In all calculations the effective interaction included the core-Coulomb correction factor of the form discussed by DeVries, Satchler, and Cramer.[34] Calculations were performed in both the post and prior formalisms and were in agreement to better than 2% when the correction factor was used. Unless otherwise noted in the text, the bound-state wave functions were computed using the conventional separation energy prescription. The optical-model parameters listed in Table II were used in both the entrance and exit channels, unless otherwise specified. In PTOLEMY the expression for the

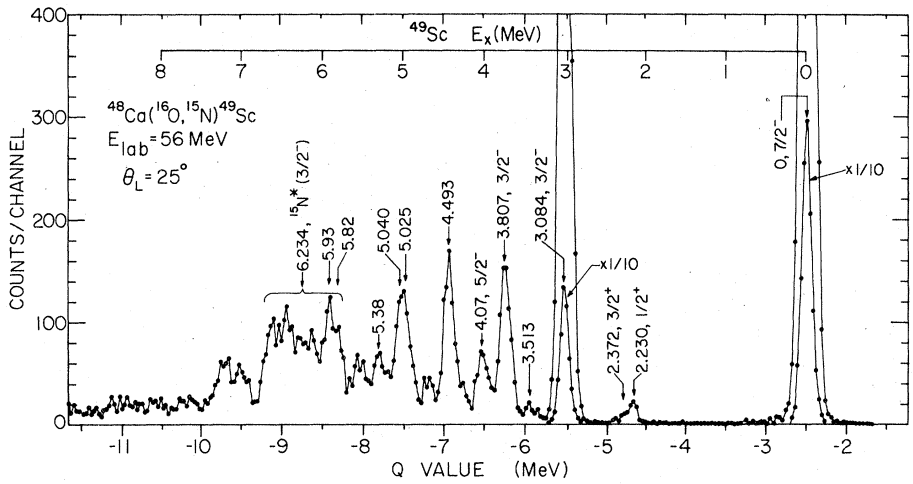

FIG. 12. Excitation spectrum obtained for the $^{48}Ca(^{16}O, ^{15}N)^{49}Sc$ reaction using the magnetic spectrograph.

differential cross section is of the form

$$\frac{d\sigma}{d\Omega}(\theta) = (C^2S)_{ab}(C^2S)_{AB}\,\sigma^{\mathrm{DWBA}}(\theta)\,,$$

where for the reaction $A(a,b)B$ the quantities $(C^2S)_{ab}$ and $(C^2S)_{AB}$ refer to the spectroscopic factors for projectile and target nuclei, respectively.

1. $^{48}Ca(^{16}O,^{15}N)^{49}Sc$

The angular distributions calculated for the $^{48}Ca(^{16}O, ^{15}N)^{49}Sc$ one-proton transfers are shown in Fig. 11. The solid curves are the predicted absolute cross sections using spectroscopic factors obtained for ^{49}Sc in studies of $(^3He, d)$ and (α, t).[31] The spectroscopic factors reported in the literature for ^{15}N differ substantially for different experiments[35,36] and in this study we took $C^2S = 2.0$ for $^{15}N_{g.s.}$ and $C^2S = 4.0$ for the $^{15}N^*(\frac{3}{2}^-, 6.33$ MeV) state. Calculations were performed with two bound-state parameter sets: (1) with $r_0 = 1.25$ fm and $a_0 = 0.65$ fm and no spin orbit term (NSO); and (2) with the same parameters as those used in the light-ion study[31] from which the spectroscopic factors for ^{49}Sc were taken (SO). These parameters are listed in Table IV. The shapes obtained in the two calculations are essentially identical although, as expected, the magnitudes change slightly.

The usual separation energy prescription was used to calculate the bound-state wave functions for all states. For the 2p-1h states at $E_x \approx 2.3$ MeV in ^{49}Sc, additional calculations were performed with bound state wave functions generated with the Pinkston-Satchler prescription.[37] This prescription results in an effective bound-state wave function which has the proper asymptotic behavior and a more nearly "correct" normalization in the interior than that obtained with the usual separation energy prescription. The curves shown in Fig. 11 are the calculations performed using no spin orbit term, and for the $(\frac{1}{2}^+ + \frac{3}{2}^+)$ doublet using the Pinkston-Satchler prescription to generate the bound-state form factor.

The shapes predicted by the calculations are on the whole in fair agreement with the data. Perhaps the largest disagreement is observed for the angular distribution for the $\frac{3}{2}^-$ state, where DWBA predicts more strength at larger angles than is observed. The spectroscopic factors used in the calculation are listed in Table V for both target and projectile. Also shown in Table V are the observed ratios of the experimental angle-integrated total cross sections, σ^{exp}, to the theoretical total cross sections, σ_{th}, calculated with the various bound-state parameter sets. The strengths predicted, $\sigma_{\mathrm{th}}^{\mathrm{SO}}$, for the $1f_{7/2}$ and $2p_{3/2}$ single-particle states are ~10% and ~40% larger, respectively, than observed. The excited $\frac{3}{2}^-$ state of ^{15}N is underpredicted by ~40%. It should be remembered, however, that the extraction of the yield for this state is somewhat uncertain because of its width and the possible presence of a background.

As mentioned previously, we were unable to extract angular distributions for the $\frac{1}{2}^+$ and $\frac{3}{2}^+$ states at 2.3 MeV separately. Calculations show that the $\frac{3}{2}^+$ strength is predicted to be ~6 times stronger than the $\frac{1}{2}^+$. This is consistent with our results obtained at several angles where the $\frac{3}{2}^+$ state is stronger by a factor of 2–5. The summed predicted angular distributions overestimated the observed cross section by some 20–40% (Table V) when the more realistic Pinkston-Satchler form

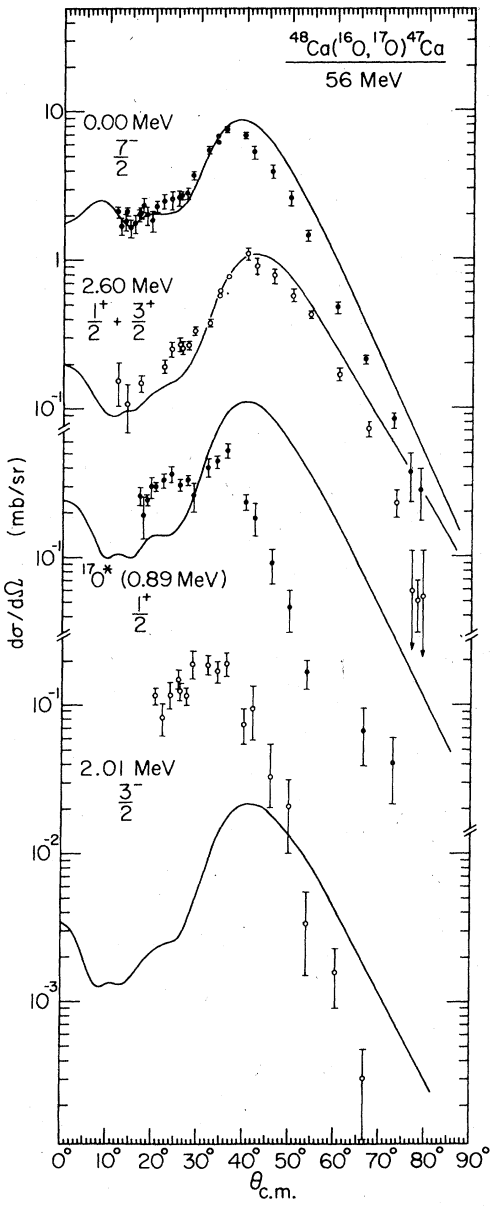

FIG. 13. Angular distributions extracted for the transfer reaction (^{16}O, ^{17}O). The solid curves are DWBA predictions using spectroscopic factors derived from light-ion studies. See text for discussion.

factor is used. When the usual separation energy form factor is used the cross section for the $\frac{1}{2}^+$ and $\frac{3}{2}^+$ states is overestimated by a factor of 4–5.

2. $^{48}Ca(^{16}O,^{17}O)^{47}Ca$

The predicted DWBA angular distributions for the ^{48}Ca(^{16}O, ^{17}O)^{47}Ca reactions are shown in Fig. 13. As for the (^{16}O, ^{15}N) reactions the solid curves represent the predicted absolute cross sections

TABLE IV. Bound-state parameters used in DWBA calculations for (^{16}O, ^{15}N) and (^{16}O, ^{17}O) transfers.

	V [a] (MeV)	r_0 (fm)	a_0 (fm)	λ	
^{49}Sc	c	1.25	0.65		NSO
	c	1.20	0.65	25	SO
^{15}N	c	1.25	0.65		NSO
	c	1.20	0.65	25	SO
^{47}Ca	c	1.25	0.65		NSO
	c	1.25	0.65	25	SO
	$\frac{7}{2}^-$ 51.07	1.25	0.65	25	PS [b]
	$\frac{3}{2}^-$ 52.00	1.39	0.65	25	
	$\frac{1}{2}^+$ 51.20	1.117	0.65	25	
	$\frac{3}{2}^+$ 52.40	1.14	0.65	25	
^{17}O	c	1.25	0.65		NSO
	c	1.25	0.65	25	SO
	c	1.25	0.65	25	PS

[a] The binding potential is of the form:

$$U(r) = -V_0 f(x) + \left(\frac{\lambda}{45.2}\right)\left(\frac{\vec{L}\cdot\vec{S}}{r}\right)V_0 \frac{d}{dr} f(x),$$

$$f(x) = [1 + \exp(x)]^{-1}, \quad x = \frac{r - r_0 A^{1/3}}{a_0}.$$

[b] These parameters were used in Ref. 38 to extract spectroscopic factors in study of (p, d) reaction.

[c] Depth established using separation energy prescription.

calculated with spectroscopic factors obtained from light-ion studies. The bound-state wave function dependence was investigated by performing calculations with (1) standard parameters (NSO), (2) parameters which include a spin-orbit term (SO), and (3) a parameter set used in analysis of (p, d) results[38] which employed the Pinkston-Satchler prescription (PS). These parameter sets are summarized in Table IV. While the predicted angular distributions calculated with the different bound-state wave functions differ in magnitude, their shapes are essentially identical. The curves shown in Fig. 13 are calculations which used the spectroscopic factors for ^{47}Ca obtained in a study of ^{48}Ca(p, d)^{47}Ca at E_{lab} = 40 MeV.[38] The spectroscopic factors for ^{17}O were taken from ^{16}O(d, p)^{17}O studies.[39,40]

In contrast to the (^{16}O, ^{15}N) reaction, the DWBA calculations do not reproduce the angular distributions observed for the (^{16}O, ^{17}O) transfers very well. While the shapes of the angular distribution for the single-hole states are still fairly well re-

TABLE V. Results of DWBA analysis of $^{48}Ca(^{16}O, ^{15}N)^{49}Sc$ reactions.

Q value (MeV)	^{49}Sc E_x	^{49}Sc J^π	^{49}Sc C^2S [a]	^{15}N E_x	^{15}N J^π	^{15}N C^2S [b]	σ_{exp} [c] (mb)	$\frac{\sigma_{exp}}{\sigma_{th}^{NSO}}$ [d]	$\frac{\sigma_{exp}}{\sigma_{th}^{SO}}$ [e]
−2.50	0.00	$\frac{7}{2}^-$	1.00	0.00	$\frac{1}{2}^-$	2.00	10.29	1.07	0.89
−4.70	2.20	$\frac{1}{2}^+$	0.09	0.00	$\frac{1}{2}^-$	2.00	0.13	0.22	0.35
−4.87	2.37	$\frac{3}{2}^+$	0.066	0.00	$\frac{1}{2}^-$	2.00		(0.67) [f]	(0.86) [f]
−5.58	3.08	$\frac{3}{2}^-$	0.703	0.00	$\frac{1}{2}^-$	2.00	4.87	0.62	0.61
−8.82	0.00	$\frac{7}{2}^-$	1.00	6.32	$\frac{3}{2}^-$	4.00	2.67	1.14	1.36

[a] Reference 31.
[b] References 35 and 36 (see text).
[c] Experimental errors ±10%.
[d] σ_{th}^{NSO} are PTOLEMY predictions using no spin orbit in bound-state calculation. See text.
[e] σ_{th}^{SO} are PTOLEMY predictions using spin-orbit term in bound-state calculations. See text.
[f] For calculations using Pinkston-Satchler prescription for bound wave function ($r_0 = 1.0$ fm). See text.

produced by the DWBA predictions, the positions of the cross section maxima are mispredicted by ≈2–5° for both angular distributions. For the $^{17}O^*(\frac{1}{2}^+)$ and $^{47}Ca(\frac{3}{2}^-)$ states the calculations describe the data very poorly. The predicted bell-shaped angular distributions are not only shifted by ~5°–10° with respect to the data, but the data at forward angles for the $^{17}O^*(\frac{1}{2}^+)$ angular distribution suggest that the overall predicted shape is in disagreement.

As can be seen in Table VI the predicted strengths, σ_{th}^{PS}, for the single-hole states are in agreement with experiment to within ~20%. In the case of the experimental level at $E_x = 2.6$ MeV, DWBA predicts that the transfer to the $1d_{3/2}$ single-particle orbital dominates [i.e., $\sigma(\frac{3}{2}^+) \approx 3\sigma(\frac{1}{2}^+)$].

The predicted strengths for the $^{17}O^*(\frac{1}{2}^+)$ and $^{47}Ca(\frac{3}{2}^-)$ states, however, are in much poorer agreement with the data. The excited $^{17}O^*(\frac{1}{2}^+)$ state is predicted to be about 2 times stronger than observed, while the $^{47}Ca(\frac{3}{2}^-)$ 1p-2h state is underestimated by a factor of 6. In the case of the $^{47}Ca(\frac{3}{2}^-)$ state, the spectroscopic factors extracted for this level in the various light-ion studies differ greatly (i.e., $C^2S = 0.02$–0.12).[38,41–43] These differences are in part due to the different bound-state wave functions used. The agreement which can be obtained if these spectroscopic factors are used in shown in Table VI. The observed strength is underestimated by a factor of 2–6 depending on the particular choice of parameters and spectroscopic factors.

TABLE VI. Results of DWBA analysis of $^{48}Ca(^{16}O, ^{17}O)^{47}Ca$ reactions.

Q value (MeV)	^{47}Ca E_x	^{47}Ca J^π	^{47}Ca C^2S [a]	^{17}O E_x	^{17}O J^π	^{17}O C^2S [c]	σ_{exp} (mb)	$\frac{\sigma_{exp}}{\sigma_{th}^{NSO}}$ [d]	$\frac{\sigma_{exp}}{\sigma_{th}^{SO}}$ [d]	$\frac{\sigma_{exp}}{\sigma_{th}^{PS}}$ [d]
−5.80	0.00	$\frac{7}{2}^-$	6.7	0.00	$\frac{5}{2}^+$	0.81	10.88	1.02	0.80	0.80
−6.67	0.00	$\frac{7}{2}^-$	6.7	0.870	$\frac{1}{2}^+$	0.71	0.589	0.63	0.53	0.53
−7.81	2.01	$\frac{3}{2}^-$	0.02 (0.05–0.12) [b]	0.00	$\frac{5}{2}^+$	0.81	0.231	11.76 (5–2) [b]	10.61 (4–2) [b]	6.47
−8.39	2.590	$\frac{3}{2}^+$	3.4	0.00	$\frac{5}{2}^+$	0.81	1.624	0.49	0.53	0.84
−8.42	2.62	$\frac{1}{2}^+$	1.8	0.00	$\frac{5}{2}^+$	0.81				

[a] Spectroscopic factors from (p,d) of Ref. 38. Analysis used binding energy and PS prescriptions for bound-state wave functions (see Table IV). With the exception of the $\frac{3}{2}^-$ state (2.01 MeV) these spectroscopic factors are in good agreement with other analyses (Refs. 41, 42, and 43).
[b] Spectroscopic factors from (p,d) (d,t) and (α,He) studies of Refs. 41–43 which used separation energy prescription.
[c] Spectroscopic factors Refs. 39 and 40.
[d] See text and Table IV for definition of NSO, SO, and PS notations.

C. DISCUSSION

The data obtained for the ^{48}Ca(^{16}O, ^{15}N)^{49}Sc and ^{48}Ca(^{16}O, ^{17}O)^{47}Ca reactions provide a rather good test of reaction theory because of the different character of the states populated. Specifically, angular distributions were obtained for: (1) transfer to single-particle (hole) states, (2) transfers leaving the outgoing projectile in an excited state, and (3) transfers to states of more complex configuration (i.e., 2p-1h and 1p-2h states).

Attention has been focused on two aspects in the comparison between theory and experiment: the detailed shapes of the angular distributions and the magnitudes of the reaction strength. For the transfers to the single-particle (hole) states the overall agreement between the predicted and measured shapes and magnitudes is rather good. However, with the exception of the transition to the ^{49}Sc($\frac{7}{2}^-$) ground state, the calculated bell-shaped peaks are located at angles 2–5° larger than observed and the strength at large angles is overestimated. Such behavior has been suggested to result from polarization effects on the single-nucleon bound-state wave functions due to the proximity of the other nucleus.[44,45] It would be interesting to see if such calculations can provide an explanation of the data.

While the shape and magnitude for the angular distribution associated with the [^{15}N*($\frac{3}{2}^-$) ⊗ ^{49}Sc($\frac{7}{2}^-$) g.s.] transfer are rather well reproduced by DWBA, the angular distribution for the [^{17}O*($\frac{1}{2}^+$) ⊗ ^{47}Ca ($\frac{7}{2}^-$) g.s.] is poorly fitted both in shape and magnitude. Analyses[27,46,47] of other reactions have shown that, depending on kinematics and nuclear structure, multistep processes may contribute significantly to transfer processes and strongly influence the magnitude and shapes of the angular distributions. There are several inelastic two-step and sequential processes (e.g., [^{16}O, ^{17}O($\frac{5}{2}^+$)] → [^{17}O($\frac{5}{2}^+$), ^{17}O*($\frac{1}{2}^+$)] and [^{16}O, ^{18}O(0^+, 2^+)] → [^{18}O(0^+, 2^+), ^{17}O*($\frac{1}{2}^+$)]) which may be important; however, detailed calculations are needed to see whether these can reproduce the observed angular distribution, and also explain why the ^{15}N*($\frac{3}{2}^-$) angular distribution is not anomalous.

A similar situation exists for the angular distribution to the 1p-2h state at $E_x = 2.016$ MeV in ^{47}Ca. While the angular distribution for the 2p-1h states in ^{49}Sc is adequately reproduced by DWBA, the angular distribution associated with the 1p-2h state in ^{47}Ca is poorly predicted; in particular, the strength is underestimated by a factor of 2–6. There are several possible explanations: (1) A more realistic form factor is needed; (2) inelastic-two-step processes (e.g., [^{48}Ca(^{16}O, ^{16}O)^{48}Ca*(2^+)] → [^{48}Ca*(2^+)(^{16}O, ^{17}O)^{47}Ca($\frac{3}{2}^-$)]) contribute; or (3) sequential processes (e.g., [^{48}Ca(^{16}O, ^{18}C)^{46}Ca(0^+, 2^+)] → [^{46}Ca(0^+, 2^+)(^{18}O, ^{17}O)^{47}Ca($\frac{3}{2}^-$)]) are important. While detailed calculations are needed to assess the situation, some comments can be made at this time. Regarding explanation (1), studies with (p,d) and (α,t) reactions[41,43] show that there are significant neutron 2p-2h admixtures in the ^{48}Ca ground state whose inclusion in a microscopic form factor calculation could provide an explanation of the observed discrepancy. Regarding explanation (2), in the discussion of the inelastic scattering results (Sec. V B) it was seen that within a macroscopic one-step description the nuclear and Coulomb deformations are different. Together with the light-ion transfer results[38,41–43] this strongly suggests that neutron configurations are involved. Therefore the parentage for inelastic two step could be quite large and provide an important route. In regard to explanation (3) the sequential two-step process forms a two-hole state in the first step and a 1p-2h state in the second. The parentages for these two processes are large and therefore they may be important.

The anomalous behavior of the transfer to the 1p-2h state in ^{47}Ca becomes particularly interesting in view of the observation that the transfer to the 2p-1h states in ^{49}Sc via (^{16}O, ^{15}N) appears to be in reasonable agreement with DWBA. It is our belief that an understanding of this behavior will give information regarding the nature of multistep processes in heavy-ion reactions and their sensitivity to the detailed structure of the nuclei involved. Thus far preliminary calculations[48] for the population of the 2p-1h states in ^{49}Sc via the (^{16}O, ^{15}N) reaction have indicated that these transitions proceed primarily via one-step processes, as suggested also by the success of the present DWBA analysis. Calculations for the 1p-2h state in ^{47}Ca would be of great interest.

VII. TWO-NUCLEON TRANSFERS

A. RESULTS

1. ^{48}Ca(^{16}O,^{14}C)^{50}Ti and ^{48}Ca(^{16}O,^{18}O)^{46}Ca

The experimental results and DWBA analysis for the (^{16}O, ^{18}O) reaction and for most of the (^{16}O, ^{14}C) transitions studied have already been presented in detail in Ref. 50. In the present paper we include the data as well as a brief summary of some of the discussion in Ref. 50, for the sake of completeness in establishing the trends of the transfer reactions on ^{48}Ca. The spectra obtained at $\theta_{lab} = 25°$ for the ^{14}C and ^{18}O channels are shown in Figs. 6 and 4, respectively. The levels labeled in the spectra are those for which angular distributions were extracted. In the two-neturon pickup reaction, transitions populating the excited (2^+ and 4^+) states of ^{18}O are particularly strong. As

TABLE VII. Levels populated in ^{50}Ti in the (^{16}O, ^{14}C) reaction and their cross sections compared with those observed in (^3He,n) measurements.

^{50}Ti		(^{16}O, ^{14}C) present work			(^3He,n) [b]
E_x [a] (MeV)	J^π	Q value (MeV)	σ_{exp} (mb)	$\frac{d\sigma^{max}}{d\Omega}(\theta)$ (mb/sr)	$\frac{d\sigma^{max}}{d\Omega}(\theta)$ (mb/sr)
0.00	0^+	−0.54	0.370	1.60(7°)	0.40(0°)
1.55	2^+	−2.09	0.480	2.20(6°)	0.08(20°)
2.68	4^+	−3.22	0.340	0.80(6°)	
3.20	6^+	−3.74	0.110	0.22(14°)	
	•				
	•				
	•				
4.18	(2^+) [c]	−4.80	0.570	1.50(6°)	0.10(15°) [d]
4.32	(2^+)				
	•				
	•				
	•				
4.80	$(2^+,4^+)$	−5.34	0.260	1.30(5°)	
	•				
	•				
	•				
5.42	(4^+) [c]	−5.96	0.180	0.55(8°)	
	•				
	•				
	•				
5.85	$(2^+,4^+)$ [c]	−6.39	0.390	1.50(7°)	
	•				
	•				
	•				
7.19	0^+	−7.73	0.270	0.70(7°)	0.27(0°)

[a] Only levels of ^{50}Ti identified in (^{16}O, ^{14}C) spectra are listed.
[b] Reference 49.
[c] L assignments based on shapes of angular distributions in (^{16}O, ^{14}C). See text.
[d] In Ref. 49 this level has $E_x = 4.44$ MeV and $J^\pi = (2^+)$.

TABLE VIII. Levels in ^{46}Ca and ^{18}O excited in the (^{16}O, ^{18}O) reaction and their cross sections compared with those observed in (p,t) studies.

	(^{16}O, ^{18}O) present work						(p,t) [b]
	^{46}Ca		^{18}O				
Q value [a] (MeV)	E_x (MeV)	J^π	E_x (MeV)	J^π	σ (mb)	$\frac{d\sigma^{max}}{d\Omega}(\theta)$ (mb/sr)	$\frac{d\sigma^{max}}{d\Omega}(\theta)$ (mb/sr)
−5.04	0.00	0^+	0.00	0^+	0.190	0.30(12°)	2.607(13°)
−6.39	1.35	2^+	0.00	0^+	0.033	0.05(19°)	0.579(25°)
	2.424	0^+					0.107(13°)
	2.575	(4^+)					0.131(48°)
	2.975	(6^+)					0.067(70°)
	3.021	2^+					0.047(28°)
	3.615	3^-					0.079(38°)
	3.642	(2^+)					
−7.02	0.00	0^+	1.98	2^+	0.233	0.25(15°)	
−8.59	0.00	0^+	3.55	4^+	0.224	0.27(13°)	

[a] Listed are the Q values of the identified groups.
[b] Reference 54.

explained in Ref. 50, the Doppler-broadened peak near 3.5 MeV excitation in the (^{16}O, ^{18}O) spectrum was assumed to arise solely from the transition to the 4$^+$ state of ^{18}O despite ambiguity in resolving this level from several other possible transitions of similar Q value.

The levels populated in the present (^{16}O, ^{14}C) and (^{16}O, ^{18}O) reactions, and their relative strengths, are compared in Tables VII and VIII with analogous results from the (^{3}He, n) (Ref. 49) and (p, t) (Ref. 54) reactions. While both the light-ion and heavy-ion induced two-nucleon transfers exhibit a high degree of selectivity in populating states of the residual nucleus, there are significant differences in the selectivity, which can be traced to differences in kinematic matching conditions. For example, the (^{3}He, n) reaction shows a strong preference for low L-transfer ($L = 0$ or 2), while (^{16}O, ^{14}C) shows no such restriction. On the other hand, the heavy-ion reactions populate sharp states over a much narrower region of excitation energy than do their light-ion counterparts. Thus, the (^{3}He, n) reaction strongly and selectively populates states in ^{50}Ti up to 15–20 MeV excitation. In contrast, the (^{16}O, ^{14}C) spectrum above $E_x \approx 7$ MeV shows no evidence of selective population of individual states, but rather appears to arise from either (1) population of many closely spaced levels in ^{50}Ti, (2) population of Doppler-broadened levels in ^{14}C which congest the energy spectrum, or (3) some other mechanism [e.g., (^{16}O, ^{15}N* → ^{14}C + p)] which gives rise to a continuum energy distribution.

The angular distributions for the (^{16}O, ^{14}C) transitions are shown in Fig. 14, and for (^{16}O, ^{18}O) in Fig. 15. The forward-angle oscillatory pattern which provides a signature of the L transfer in the (^{16}O, ^{14}C) distributions has been discussed previously.[28,30] Similar oscillations are observed for the (^{16}O, ^{18}O) transitions leaving ^{18}O in its ground state, but appear damped out in the angular distributions corresponding to population of excited states of ^{18}O. The angle-integrated two-nucleon transfer cross sections [even for the rather well-matched (^{16}O, ^{14}C) transitions] are generally a factor of ~10 weaker than the single-nucleon transfers (see Table I).

2. ^{48}Ca(^{16}O, ^{14}N)^{50}Sc

The spectrum obtained at $\theta_{lab} = 25°$ for the ^{14}N channel is shown in Fig. 5. Because of the density of levels in ^{50}Sc and the weak strength of the transfers, positive identification and extraction of the angular distributions were difficult. The spectra obtained with the spectrograph show that the group near the ground state has approximately equal contributions from the ^{50}Sc(5$^+$) ground state, and the ^{50}Sc(3$^+$) state at 0.330 MeV. In the TOF measurements a separation between contributions at $E_x \approx 0.00$ MeV and $E_x \approx 0.300$ MeV could be observed at most angles and angular distributions for these two groups were extracted. Angular distributions were also extracted for the transfers to the ^{50}Sc(4$^+$) state at 0.756 MeV and the ^{50}Sc(1$^+$) state at 1.854 MeV. At higher excitation the spectrum becomes too complex for unambiguous identification of levels. In Fig. 5 the expected locations of the ^{14}N excited states at $E_x = 2.31$ MeV (0$^+$) and $E_x = 3.95$ MeV (1$^+$) are indicated and as can be seen in the figure there are groups at these energies. However, as can be seen in Table IX these energies are also consistent with states in ^{50}Sc and unambiguous identification is not possible based on these measurements.

The levels populated in the (^{16}O, ^{14}N) reaction are compared with those observed in the (^{3}He, p) (Refs. 51 and 52) and (α, d) (Ref. 53) reactions in Table IX. Similar conclusions can be drawn from this comparison as are drawn from a comparison of the (^{16}O, ^{14}C) and (^{3}He, n) reactions, a strong selectivity in the levels populated by all these reactions with quite different preferences in optimum L transfer and Q value. The level selectivity appears correlated with the structure of the states excited, while the preferences in L space and energy space are determined by the kinematics of the different reactions.

The angular distributions extracted for the (^{16}O, ^{14}N) reactions are shown in Fig. 16. The angular distributions appear to be smooth within errors and peaked at forward angles, with some indication of a slight enhancement of strength near the grazing angle. The angle-integrated cross sections are of the same order of magnitude as for the other two-nucleon transfers.

B. DWBA analysis

The DWBA analysis presented here for the two-nucleon transfers was carried out under the assumption of a cluster transfer. A detailed analysis for the two-proton and two-neutron transfers was already presented in Ref. 50, where microscopic calculations for the 0$^+$-0$^+$ transitions were also performed.

In the cluster transfer calculations it was assumed that the interaction which causes the transfer acts on the center of mass of a correlated pair of nucleons in an intrinsic 0s state. In the (^{16}O, ^{14}C) and (^{16}O, ^{18}O) calculations the transferred pairs are thus characterized by a single intrinsic state, of spin $S = 0$ and isospin $T = 1$, and the predicted transfer cross section can consequently be factorized, in the conventional manner, into a part containing the reaction dynamics and a pro-

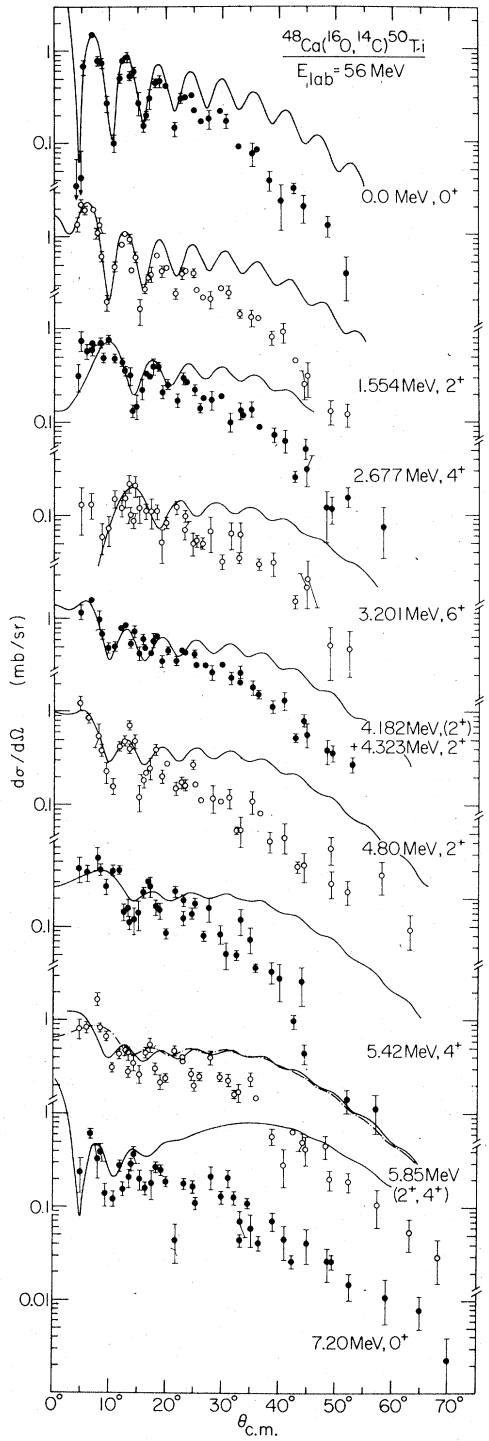

FIG. 14. Angular distributions extracted for the (^{16}O, ^{14}C) reaction. The solid curves are DWBA calculations using optical-model parameters in Table II. The DWBA calculations are normalized to fit the forward-angle data.

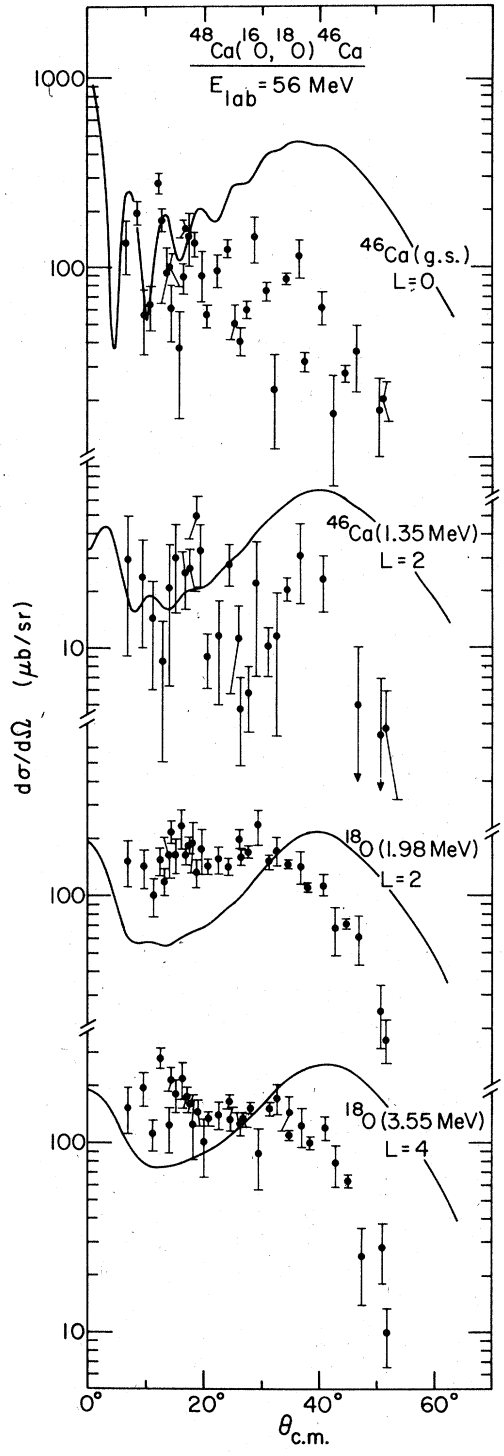

FIG. 15. Angular distributions extracted for the $^{48}Ca(^{16}O, ^{18}O)^{46}Ca$ reaction. The solid curves are DWBA calculations using the optical-model parameters of Table II in both entrance and exit channels. The DWBA calculations are arbitrarily normalized.

TABLE IX. Levels populated in ^{50}Sc in the (^{16}O, ^{14}N) reaction and their cross sections compared with those observed in (^{3}He,p) and (α,d) reactions.

^{50}Sc		(^{16}O, ^{14}N) [b]			(^{3}He, p) [c]	(α,d) [d]
E_x [a] (MeV)	J^π	Q value (MeV)	σ (mb)	$\frac{d\sigma^{max}}{d\Omega}(\theta)$ (mb/sr)	$\frac{d\sigma^{max}}{d\Omega}(\theta)$ (mb/sr)	$\frac{d\sigma^{max}}{d\Omega}(\theta)$ (mb/sr)
0.00	5^+	−6.85	0.147	0.40(5°)	0.06(30°)	0.70(20°)
0.258	2^+				0.08(20°)	
0.330	3^+	−7.15	0.089	0.15(7°)	0.14(20°)	0.20(20°)
0.756	4^+	−7.61	0.032	0.12(6°)	0.02(35°)	0.06(20°)
1.854	1^+	−8.70	0.023	0.05(6°)	1.00(7°)	0.18(32°)
2.227	(3^+)				0.12(2°)	0.10(20°)
2.331	(4^+)				0.04(35°)	0.10(20°)
3.090	0^+				0.40(5°)	
3.259	(2^+)					
3.287					0.30(15°)	
3.497					0.04(10°)	
3.617					0.10(10°)	
3.682					0.20(5°)	
3.731						
3.943	$(2^+, 3^+)$				0.18(10°)	

[a] Reference 52.
[b] Present work.
[c] Reference 51.
[d] Reference 53.

duct of spectroscopic factors. Such a factorization is not possible without further assumptions for the (^{16}O, ^{14}N) reaction, since here an additional intrinsic state of the transferred pair, with $S = 1$, $T = 0$, is possible. Even if one confines consideration to the latter ("deuteron") intrinsic state, more than one center-of-mass bound state is required to give a full description of the unnatural-parity states populated. The cross section is then a coherent sum involving the several bound-state wave functions, each weighted by its associated spectroscopic amplitude. Such calculations have not been performed here. We have included for each (^{16}O, ^{14}N) transition only a single center-of-mass bound state for ^{14}N and ^{50}Sc which, based on shell-model and kinematic considerations, should provide the dominant contribution to the cluster transfer. It is believed that the (^{16}O, ^{14}N) angular distribution shapes obtained in the present "deuteron-transfer" calculations would not be greatly altered in more complete cluster-transfer calculations.

The calculations performed under the above assumptions are represented by the curves in Figs. 14–16. The bound-state wave functions were calculated in a conventional Woods-Saxon potential ($r_0 = 1.25$ fm, $a = 0.65$ fm) using the separation-energy prescription. The curves have been individually normalized to the data at the angles deemed most appropriate for each transition. The required normalization factors greatly exceed the spectroscopic factors expected from harmonic-oscillator shell-model calculations in most cases.[50] The calculated angular distribution shapes reproduce adequately the oscillatory pattern observed at far-forward angles for the (^{16}O, ^{18}O) ground-state and (^{16}O, ^{14}C) transitions, but fail to reproduce other features apparent in the measurements. Most notable is the universal overestimate in the calculations of the strength near the grazing angle relative to that at more forward angles. A related problem is the inability to predict the observed persistance of oscillations at large angles, e.g., for the (^{16}O, ^{18}O) ground-state transition. The calculated angular distributions are sensitive to bound-state parameters; however, unreasonable changes in bound-state radii are needed to produce angular distributions which begin to resemble the measurements.

C. Discussion

Several previous studies[50,58,59] have focused on attempting to understand the systematic discrepancies observed here and elsewhere between measured two-nucleon transfer angular distributions and conventional DWBA calculations. In these studies it was noted that, by empirically modifying optical-model parameters, fits to the shapes of the angular distributions can be obtained. While qualitative arguments can be advanced to provide some explanation for this behavior,[50] the adjustment of optical-model parameters must be viewed as an *ad hoc* procedure. The procedure does have the merit, however, of being able to reproduce the observed shapes of a surprisingly large num-

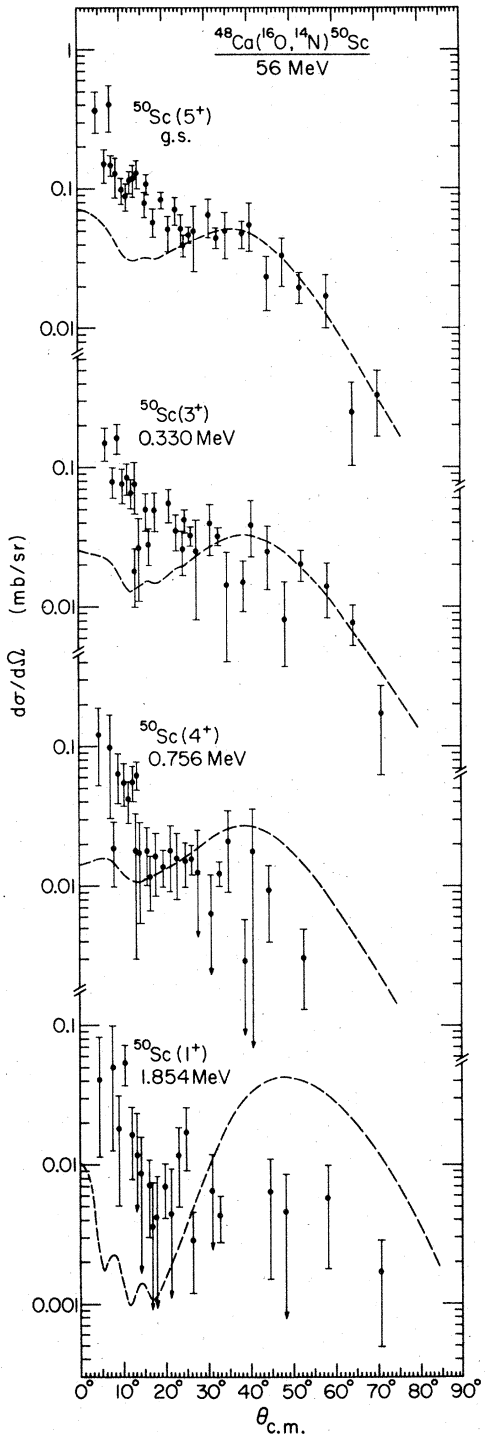

FIG. 16. Angular distributions extracted for the $^{48}Ca(^{16}O,^{14}N)^{59}Sc$ reaction. The dashed curves are DWBA predictions with the assumptions discussed in the text. The curves are arbitrarily normalized.

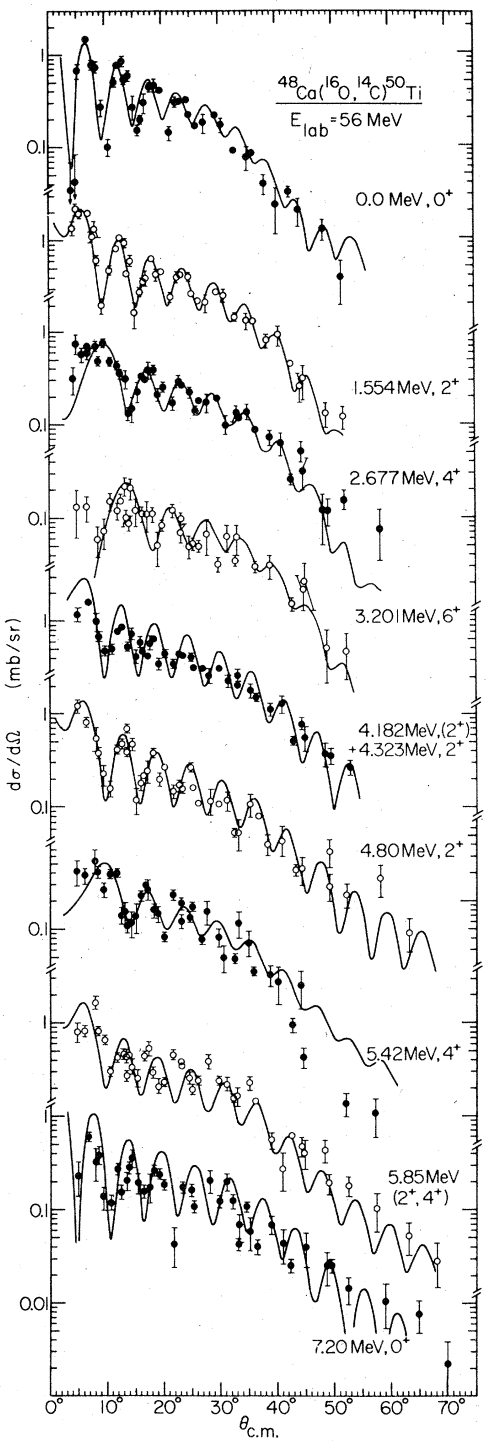

FIG. 17. Angular distributions extracted for the $^{48}Ca(^{16}O,^{14}C)^{50}Ti$ reaction. The solid curves are DWBA calculations using modified optical-model parameters in the exit channel. The curves are normalized to obtain the best fit.

ber of transfers, and moreover of focusing attention on some of the features in the experimental angular distributions which might otherwise be overlooked.

For example, shown in Figs. 17 and 18 are the angular distributions for the (^{16}O, ^{14}C) and (^{16}O, ^{18}O) transfers together with DWBA calculations using a modified but consistent set of optical-model parameters. (In the calculations shown, the real diffuseness for the exit-channel optical model has been set to 0.7 fm, and a radial cutoff at $R = 8.0$ fm has been employed.) The calculations reproduce the observed behavior rather well for essentially all the transfers.

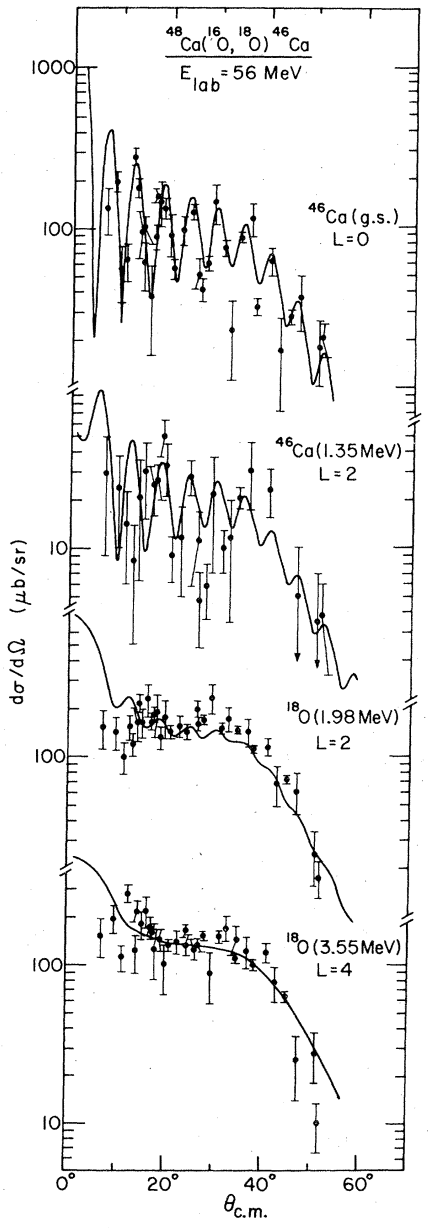

FIG. 18. Angular distributions extracted for the ^{48}Ca(^{16}O, ^{18}O)^{46}Ca reaction. The solid curves are DWBA calculations using modified-model optical parameters in the exit channel. The curves were normalized to obtain the best fit to the data.

Several features in the experimental angular distributions become rather obvious when these modified DWBA calculations are compared with the data. First, as is most clearly evident in the (^{16}O, ^{14}C) angular distributions for the transfers to the 0^+, 2^+, 4^+, and 6^+ states in ^{50}Ti, the oscillatory patterns at forward angles are a clear signature of the L transfer.[28] Second, as illustrated in the (^{16}O, ^{18}O) transfers, the shapes of the angular distributions are quite sensitive to the detailed bound-state wave functions. Notably, the $L = 2$ transfers to the ^{46}Ca(2^+) state and ^{18}O*(2^+) state are seen to exhibit different shapes, although the poor statistics for the ^{46}Ca(2^+) state tend to obscure the differences. The differences can be understood in the framework of DWBA as resulting from the different localization in l space. This localization in l space is strongly dependent on the rate of falloff of the bound-state wave functions beyond the nuclear surface.[50]

Several studies have discussed more sophisticated theoretical calculations for some of the (^{16}O, ^{14}C) and (^{16}O, ^{18}O) transfers presented here.[50,60,61] For example, Eisen *et al.*[50] have performed DWBA calculations using microscopic form factors[62] (for the $L = 0$ transfers) as well as cluster-model form factors. Using modified optical-model parameters the following results were found: (1) The calculations using cluster-model or microscopic form factors predict essentially the same shapes for the angular distributions; (2) the *relative* spectroscopic factors obtained using the cluster model for the ^{18}O(0^+, 2^+, and 4^+), ^{46}Ca(0^+ and 2^+), and ^{50}Ti(0^+, 2^+, and 6^+) states were on the whole in reasonable agreement with those extracted in light-ion studies, and also with those predicted using the harmonic-oscillator (HO) prescription; (3) the *absolute* cross sections predicted using HO spectroscopic amplitudes underestimate the observed strengths by factors of 2–1000 depending on the transitions. While the somewhat successful prediction of the relative spectroscopic factors is encouraging, the large discrepancy in the absolute magnitudes and the shapes (without optical-model modification) between the calculated angular distributions and the measured ones is the most striking. Such discrepancies had been noted previously in similar studies.[62] In the analysis of the (^{16}O, ^{18}O) and (^{16}O, ^{14}C) transfers by Feng, Udagawa, and Tamura,[60] the effect of using more

realistic microscopic form factors and the importance of two-step sequential processes were investigated. The shapes of the angular distributions obtained in their calculations are very similar to those obtained with the simple cluster model. On the other hand, Feng *et al.* found that with the modified optical-model parameters of Ref. 50 the absolute magnitude of the cross section was predicted to within a factor of 2 for a great majority of the transfers studied. This agreement was due in part to the improved microscopic form factors used in the one-step process. But to a larger extent this agreement was due to the significant strength predicted for the two-step sequential transfer, which in many cases was as strong or stronger than the one-step transfer of a pair of correlated nucleons. The role of inelastic two-step processes, for which calculations have not been performed, is also of interest. Such coupled-channels calculations for two-nucleon transfers have been performed for other systems[27,46,47] and show that the contributions of inelastic two-step processes often significantly alter the shapes of the predicted angular distributions.

VIII. THREE NUCLEON TRANSFERS

A. Results

1. $^{48}Ca(^{16}O,^{13}C)^{51}Ti$

The spectrum obtained at $\theta_{lab} = 25°$ for the ^{13}C channel is shown in Fig. 6. The groups labeled were identified as levels in ^{51}Ti and ^{13}C and angular distributions were extracted. Because of the energy resolution of the TOF system, the density of levels, and the weak strength of these transfers, uncertainties exist in the assignments and the angular distributions extracted. The energy levels in ^{51}Ti and ^{13}C are listed in Table X together with the identifications made in the (^{16}O, ^{13}C) reaction. No ambiguity exists for the $^{51}Ti(\frac{3}{2}^-)$ ground state. In the region corresponding to 1.20–1.60 MeV excitation energy in ^{51}Ti three levels are known: a $\frac{1}{2}^-$ state (1.160 MeV), a $\frac{7}{2}^-$ state (1.429 MeV), and a $(\frac{5}{2}^-, \frac{7}{2}^-)$ state (1.559 MeV). In this energy region we observe what appears to be a doublet. The association of the lower excitation peak with the $\frac{1}{2}^-$ state is rather clear. Based on the observed energy of the higher excitation peak over the full angular range it appears that the major contribution to it is from the state at 1.559 MeV, although this identification is by no means certain. The group at $E_x \approx 2.15$ MeV corresponds to the region of the known 2.136 and 2.189 MeV levels; we cannot distinguish between the two. The remaining two groups near $E_x = 3.1$ and 3.7 MeV may correspond either to excited states in ^{51}Ti with ^{13}C in its ground state, or to ^{51}Ti in its ground state with ^{13}C in its excited states. At higher excitation, as for the ^{14}C channel, there is significant strength, but with our resolution it is not possible to identify levels, or even to determine whether there are many closed spaced levels or a smooth background.

TABLE X. Levels in ^{51}Ti identified in the $^{48}Ca(^{16}O, ^{13}C)$-^{51}Ti reaction.

	^{51}Ti		^{13}C		
Q value [a] (MeV)	E_x (MeV)	J^π	E_x (MeV)	J^π	σ (mb)
−2.35	0.00	$\frac{3}{2}^-$	0.00	$\frac{1}{2}^-$	0.042
−3.51	1.160	$\frac{1}{2}^-$	0.00	$\frac{1}{2}^-$	0.034
−3.85	1.429	$\frac{7}{2}^-$	0.00	$\frac{1}{2}^-$	0.040
	1.559	$(\frac{5}{2}^-, \frac{7}{2}^-)$			
−4.50	2.136	$(\frac{5}{2}^-, \frac{7}{2}^-)$	0.00	$\frac{1}{2}^-$	0.128
	2.189	$(\frac{3}{2}^-)$			
	2.69	$\frac{7}{2}^-$			
	2.896	$\frac{1}{2}^-, \frac{3}{2}^-$			
−5.51 [b]	3.164	$\frac{1}{2}^-, \frac{3}{2}^-$	0.00	$\frac{1}{2}^-$	0.058 [b]
−6.11 [b]	3.759	$\frac{9}{2}^+$	0.00	$\frac{1}{2}^-$	0.231 [b]
(−5.43) [b]	0.00	$\frac{3}{2}^-$	3.08	$\frac{1}{2}^+$	(0.058) [b]
(−6.03) [b]	0.00	$\frac{3}{2}^-$	3.68	$\frac{3}{2}^-$	(0.231) [b]

[a] Listed are the Q values of the groups identified.
[b] The levels at $E_x \approx 3.15$ and 3.70 MeV are consistent with the identification as excited levels in ^{51}Ti or excited levels in ^{13}C.

The angular distributions extracted for the six groups discussed are shown in Fig. 19. The angular distribution associated with the $^{51}Ti(\frac{3}{2}^-)$ ground state shows a pronounced oscillatory structure despite the poor statistics. The other angular distributions extracted have such large error bars and fluctuations that little information other than the presence of forward peaking and the angle-integrated strengths (see Table X) can be obtained.

The calculations shown in Fig. 19 were performed under the assumption of a cluster transfer using bound-state wave functions computed in the usual separation-energy prescription ($r_0 = 1.25$ fm, and $a = 0.65$ fm). No attempt to predict the magnitude was made and the DWBA angular distributions shown in Fig. 19 were arbitrarily normalized to best reproduce the data. As can be seen in the figure the predicted shapes are roughly consistent with the data. For the $^{51}Ti(\frac{3}{2}^-)$ ground-state transfer the calculated angular distribution does exhibit oscillator behavior, but the structure appears to be out of phase with the data. Such out-of-phase behavior has been observed in other

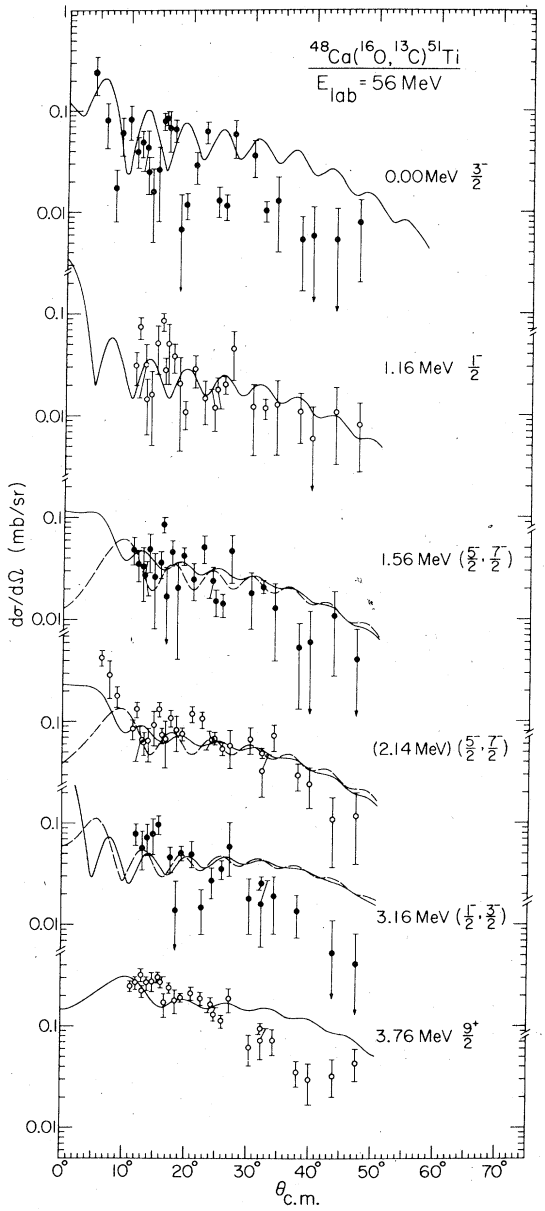

FIG. 19. Angular distributions extracted for the $^{48}Ca(^{16}O, ^{13}C)^{51}Ti$ reaction. The solid curves are DWBA calculations using the optical-model parameters of Table II in both the entrance and exit channels. The dashed curves represent the predictions for the larger spin assignment in each case. The curves are normalized so as to obtain the best fit to the data.

reactions [e.g., $^{40,42,44}Ca(^{13}C, ^{14}N)^{39,41,43}K$] (Ref. 63) and the theoretical attempt[64] to understand this phenomenon suggests that inelastic two-step processes may provide the explanation. It is also interesting to note that in a recent paper, Kubono *et al.*[65] seem to account successfully for a similar phase discrepancy observed in the angular distribution of the (^{19}F, ^{16}O) three-nucleon transfer reaction by including spin-orbit effects in the entrance- and exit-channel optical potentials.

2. $^{48}Ca(^{16}O,^{13}B)^{51}V$

The three-proton stripping reaction (^{16}O, ^{13}B) is weak and a meaningful spectrum was obtained only after the yields measured at several angles were summed (see Fig. 7). Despite the poor statistics, groups are observed at Q values consistent with excitation of low-lying levels in ^{51}V. Noted in Fig. 7 are the location of levels in ^{51}V together with the first excited state in ^{13}B. The known states in ^{51}V are compared with the levels populated in Table XI. As discussed previously[66] the reaction appears to be populating all the low-lying states in ^{51}V which are predominantly of $(f_{7/2})^3$ character. No meaningful information about the angular distributions other than their forward peaked character and their rough average strength was obtained.

3. $^{48}Ca(^{16}O,^{19}O)^{45}Ca$

The yields for the ^{19}O channel are also so small that a meaningful spectrum was not obtained at a single angle. The spectrum shown in Fig. 4 was obtained after spectra measured at several angles were summed. Indicated in the figure are the locations of known low-lying levels in ^{45}Ca and ^{19}O. Despite the poor statistics the data show that the ground state and/or the first excited state in ^{45}Ca are populated most strongly in this three-neutron

TABLE XI. Suggested identification of levels populated in $^{48}Ca(^{16}O, ^{13}B)^{51}V$ reactions.

	^{51}V		^{13}B		
Q value[a] (MeV)	E_x (MeV)	J^π	E_x (MeV)	J^π	σ (mb)
−13.32	0.00	$\frac{7}{2}^-$	0.0	$\frac{3}{2}^-$	≤0.007
−13.64	0.320	$\frac{5}{2}^-$	0.0	$\frac{3}{2}^-$	*[b]
	0.929	$\frac{3}{2}^-$	0.0	$\frac{3}{2}^-$	
−14.93	1.609	$(\frac{11}{2}^-)$	0.0	$\frac{3}{2}^-$	*
−15.13	1.813	$(\frac{9}{2}^-)$	0.0	$\frac{3}{2}^-$	*
−15.73	2.409	$(\frac{3}{2}^-)$	0.0	$\frac{3}{2}^-$	*
	2.545	$\frac{1}{2}^+$	0.0	$\frac{3}{2}^-$	
	2.675		0.0	$\frac{3}{2}^-$	
	2.699	$(\frac{3}{2}^+)$	0.0	$\frac{3}{2}^-$	
	2.790		0.0	$\frac{3}{2}^-$	
	0.00	$\frac{7}{2}^-$	3.48	$(\frac{1}{2},\frac{3}{2},\frac{5}{2})^+$	

[a] Listed are Q values for the group identified.

[b] The symbol * indicates a group was observed at that Q value.

pickup reaction.[66] Because of the small cross sections no angular distribution information, except that the strength is forward peaked, was obtained from this study.

B. Discussion

The three-nucleon transfers for which the yields were sufficient to obtain spectra were the (^{16}O, ^{13}C), (^{16}O, ^{13}B), and (^{16}O, ^{19}O) reactions, which in the simplest picture correspond to transfer of ^3He, $3p$, and $3n$ "clusters." The strongest of these, the (^{16}O, ^{13}C) transfers, are observed to have cross sections about 100–200 times weaker than observed in inelastic scattering and the single-nucleon transfers. The estimates for the three-neutron and three-proton transfers indicate that their strengths are approximately 10 times weaker than the (^{16}O, ^{13}C) transfers.

Despite their weakness, the three-nucleon transfers, as do the two nucleon transfers, demonstrate a strong selectivity. While the (^{16}O, ^{13}C) spectrum is rather complex, the (^{16}O, ^{13}B) and (^{16}O, ^{19}O) spectra at first glance seem simple. Namely, the dominant configuration expected $[^{48}Ca^*(f_{7/2})^3]$ and $[^{48}Ca^*(f_{7/2}^{-1})^3]$ for the (^{16}O, ^{13}B) and (^{16}O, ^{19}O) reactions, respectively, appear to be populated most strongly in these reactions. The observation of these levels to the exclusion of others is significant, but does not in itself distinguish between possible reaction mechanisms; e.g., three-nucleon simultaneous transfer versus sequential transfer.

IX. FOUR AND FIVE-NUCLEON TRANSFERS

1. $^{48}Ca(^{16}O,^{12}C)^{52}Ti$

The spectrum obtained for the (^{16}O, ^{12}C) reaction is shown in Fig. 6. This channel is particularly difficult to study because of the large ^{12}C yield from the carbon backing which tends to obscure the contributions from ^{48}Ca. While there are several low-lying levels in ^{52}Ti which are free of contaminants for most of the angular range studied, the strength of the four-nucleon transfer to these levels is very weak (<10 μb/sr). As labeled in Fig. 6 three low-lying states, the $^{52}Ti(0^+)$ ground state, the $^{52}Ti(2^+)$ state at 1.045 MeV, and the $^{52}Ti(2^+, 2)$ doublet at ≈2.35 MeV, were observed at several angles, but no angular distributions were extracted. It should be noted that at large angles, where no contaminant lines are present, the shape of the energy distribution is similar to ^{13}C and ^{14}C and the strength of the ^{12}C channel is large compared to ^{13}C and ^{14}C.

2. $^{48}Ca(^{16}O,^{12}B)^{52}V$ and $^{48}Ca(^{16}O,^{11}B)^{53}V$

The yields for the ^{12}B and ^{11}B channels were weak and meaningful spectra were obtained only after summing the kinematically corrected spectra measured at angles over the range $9° \leq \theta \leq 25°$. The spectrum for the three-proton–one-neutron transfer (^{16}O, ^{12}B) is shown in Fig. 7. The high density of levels in ^{52}V and ^{12}B and the limited energy resolution of our system prevented identification of the levels excited. The expected locations of the six lowest-lying levels in ^{52}V and the first two excited states in ^{12}B are indicated in the figure. The strength of the ground-state group is estimated to be $\sigma \lesssim 2$ μb.

Likewise in the five-nucleon transfer (^{16}O, ^{11}B) unambiguous information concerning level population cannot be extracted from the data. The low-lying levels in ^{53}V and ^{11}B are indicated in Fig. 7. However, this information does little more than confirm that we are indeed seeing ^{11}B with kinematics consistent with the $^{48}Ca(^{16}O, ^{11}B)^{53}V$ two-body reaction. The ground-state group indicated in the figure is estimated to have a cross section $\sigma \leq 4$ μb. As can be observed from the figures, the great majority of the strength for both ^{12}B and ^{11}B is located at higher excitation in their respective residual nuclei and the ^{11}B channel is about an order of magnitude stronger than the ^{12}B channel.

X. EXOTIC TRANSFERS

A. Results

1. $^{48}Ca(^{16}O,^{16}N)^{48}Sc$

The spectrum obtained for the (^{16}O, ^{16}N) reaction is shown in Fig. 5. While the resolution does not allow for unambiguous identification of the levels populated because of the level density in both ^{48}Sc and in ^{16}N, the data do clearly show that the reaction is selective with significant strength in two groups located below 2 MeV excitation in ^{48}Sc. Measurements with the spectrograph showed that the two groups have complex structure with contributions from several transitions involving excited states of both ^{48}Sc and ^{16}N. In Table XII the levels populated in (^3He, t) (Ref. 67) and (^6Li, ^6He) (Ref. 68) reactions are compared with our results. The angular distributions for the groups near the ground state and at $E_x \approx 1.2$ MeV are shown in Fig. 20. The mechanism for the (^{16}O, ^{16}N) reaction is not clear at present. Based on results of analysis of the (^6Li, ^6He) reaction, it might be expected that the charge-exchange process is quite weak. Calculations of sequential processes such as (^{16}O, ^{15}N)(^{15}N, ^{16}N) or (^{16}O, ^{17}O)(^{17}O, ^{16}N) have not been performed. The angle-integrated cross sections for the (^{16}O, ^{16}N) groups extracted are comparable to those for the two-nucleon transfer reactions.

2. $^{48}Ca(^{16}O,^{15}C)^{49}Ti$

The spectrum for the (^{16}O, ^{15}C) reaction is shown in Fig. 6. While this reaction is rather weak there

TABLE XII. Groups observed in the (^{16}O, ^{16}N) reaction compared with results of (^{3}He,t) and (^{6}Li, ^{6}He) studies.

Q value [a] (MeV)	(^{16}O, ^{16}N) present work ^{48}Sc [b] E_x	J^π	^{16}N E_x	J^π	σ (mb)	$\frac{d\sigma^{max}}{d\Omega}$ (mb/sr)	(^{3}He,t) [c] $\frac{d\sigma^{max}}{d\Omega}$ (mb/sr)	(^{6}Li, ^{6}He) [d] $\frac{d\sigma^{max}}{d\Omega}$ (mb/sr)
−10.38	0.00	6^+	0.0	2^- [e]	0.168	0.15	0.10	0.005
	0.131	5^+	0.0	2^-			0.12	0.015
	0.252	4^+	0.0	2^-			0.20	0.010
	0.622	3^+	0.0	2^-			0.30	0.030
−11.28	1.096	7^+	0.0	2^- [e]	0.223	0.20	0.13	0.040
	1.143	2^+	0.0	2^-			0.50	
	2.521	1^+	0.0	2^-			0.40	0.150
	•							
	•							
	•							
	6.667	0^+	0.0	2^-			0.50	
	0.00	6^+	0.121	0^-				
	0.00	6^+	0.297	3^-				
	0.00	6^+	0.397	1^-				

[a] Listed are the Q values of the groups identified.
[b] Excitation energies and spin assignments as quoted in (^{3}He,t) study of Ref. 67.
[c] Reference 67.
[d] Reference 68.
[e] Spectrograph measurements indicate that the excited states of ^{16}N contribute to this strength.

are sufficiently few low-lying levels in the ^{49}Ti + ^{15}C system that unambiguous identification of the lower few levels is possible.[69] Weakly populated, but present are the $[^{49}\mathrm{Ti}(\frac{7}{2}^-)\mathrm{g.s.} \otimes {}^{15}\mathrm{C}(\frac{1}{2}^-)\mathrm{g.s.}]$ and the $[^{49}\mathrm{Ti}(\frac{3}{2}^-) \otimes {}^{15}\mathrm{C}(\frac{1}{2}^+)\mathrm{g.s.}]$ levels. More strongly populated are groups at Q values of −11.0 and −12.5 MeV which are identified as the $[^{49}\mathrm{Ti}(\frac{7}{2}^-) \otimes {}^{15}\mathrm{C}(\frac{5}{2}^+)]$ and $[^{49}\mathrm{Ti}(\frac{5}{2}^-, \frac{7}{2}^-) \otimes {}^{15}\mathrm{C}(\frac{1}{2}^+)]$ states, respectively. As can be seen in Table XIII, the group at $Q = -12.5$ MeV could possibly be identified as the population of the $[^{49}\mathrm{Ti}(\frac{3}{2}^-) \otimes {}^{15}\mathrm{C}^*(\frac{5}{2}^+)]$ state; however, based on our energy calibration the identification indicated above is preferred. These transfer processes are comparable in strength to the (^{16}O, ^{13}C) transfers which can proceed via a standard cluster transfer and whose Q matching is much more favorable. The data clearly show a strong enhancement in the population of the states of ^{49}Ti via the excited state of ^{15}C in preference to the ^{15}C ground state. Angular distributions are shown in Fig. 21.

3. $^{48}Ca(^{16}O,^{17}N)^{47}Sc$

The (^{16}O, ^{17}N) reaction is very weak and the spectrum shown in Fig. 5 was obtained by summing spectra obtained at several angles. Very little can be inferred beyond the observation that the energy spectrum is consistent with the population of low-lying levels in ^{47}Sc. No angular distributions were obtained.

B. Discussion

The data for these "exotic" transfers are of particular interest because they potentially provide information about the importance of multistep processes proceeding via sequential transfer. While such processes may be important in such transfers as (^{16}O, ^{18}O) and (^{16}O, ^{14}C), there is no direct way to establish their importance. In the case of the "exotic" reactions considered here, however, the reaction cannot proceed via transfer of a cluster and most probably proceed via a sequential process. In particular the (^{16}O, ^{16}N), (^{16}O, ^{17}N), and (^{16}O, ^{15}C) reactions correspond to (one-proton stripping–one-neutron pickup), (one-proton stripping–two-neutron pickup), and (two-proton stripping–one-neutron pickup reactions), respectively.

The only reaction for which calculations have been performed is (^{16}O, ^{15}C). Two-step sequential calculations by Udagawa, Tamura, and Low[70] considered the routes (^{16}O, ^{14}C) → (^{14}C, ^{15}C) and (^{16}O, ^{17}O) → (^{17}O, ^{15}C). The results of these calculations are shown in Fig. 21. While the statistical errors are large, the predicted shapes of the angular distributions are consistent with the data. Moreover, the calculations also predict the relative magnitudes of the transfers populating the ^{49}Ti ground

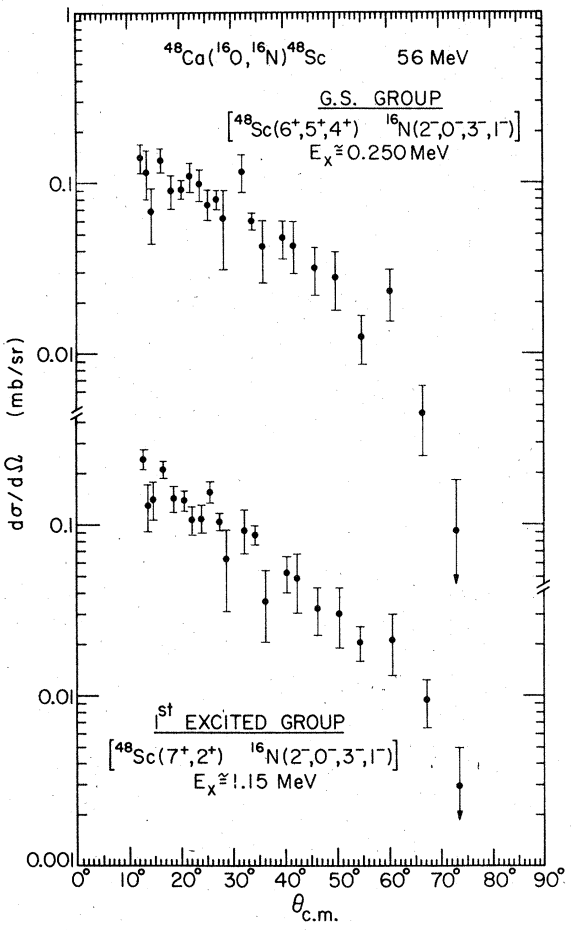

FIG. 20. Angular distributions extracted for the $^{48}Ca(^{16}O,^{16}N)^{48}Sc$ reaction.

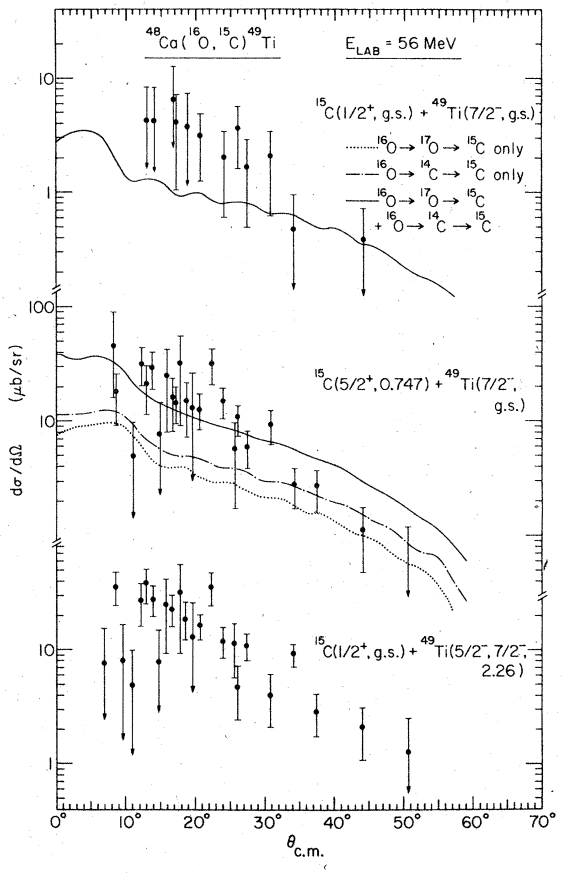

FIG. 21. Angular distribution extracted for the $^{48}Ca(^{16}O,^{15}C)^{49}Ti$ reaction. The curves shown are calculations for the sequential transfer processes indicated in the figure (Ref. 70).

TABLE XIII. Q values and levels identified in the ($^{16}O,^{15}C$) reaction. The last column lists angle-integrated cross sections.

Q values [a] (MeV)	^{49}Ti E_x (MeV)	J^π	^{15}C E_x (MeV)	J^π	σ (mb)
−10.27	0.00	$\frac{7}{2}^-$	0.00	$\frac{1}{2}^+$	0.003 ± 0.001
−11.65	1.382	$\frac{3}{2}^-$	0.00	$\frac{1}{2}^+$	≤ 0.003
	1.542	$\frac{5}{2}^- - \frac{19}{2}^-$			
	1.585	$\frac{3}{2}^-$			
	1.622	$\frac{5}{2}^- - \frac{19}{2}^-$			
	1.723	$\frac{1}{2}^-$			
	1.762				
−12.53 [b]	2.262	$\frac{5}{2}^-, \frac{7}{2}^-$	0.00	$\frac{1}{2}^+$	0.019 ± 0.004
−11.01	0.00	$\frac{7}{2}^-$	0.740	$\frac{5}{2}^+$	0.015 ± 0.003
(−12.39)	1.382	$\frac{3}{2}^-$	0.740	$\frac{5}{2}^+$	(0.019 ± 0.004)

[a] Listed are the Q values of those groups identified.
[b] The group at $Q \simeq 12.5$ MeV was identified as the $^{44}Ti(\frac{5}{2}^-, \frac{7}{2}^-)$ level. See the text.

state with ^{15}C in its ground state and first excited state. Further calculations for the other reactions would be of interest, especially in view of the calculations[60] for two-nucleon transfers which indicate that even there sequential processes may provide a sizable, and in some cases a dominant, contribution to the transition.

XI. SUMMARY AND CONCLUSIONS

In this study of ^{16}O + ^{48}Ca at E_{lab} = 56 MeV all direct reaction channels of significant strength were measured. Conventional DWBA calculations were performed for a large number of these transitions and compared with experiment. From the data alone several features are apparent:

(1) The dominating importance of kinematic matching conditions is illustrated in the selectivity of the reaction channels populated. The only channels observed with significant strength are those reactions where the kinematic matching is favorable. These correspond for the ^{16}O + ^{48}Ca system to reactions involving one or more neutron pickup and one or more proton stripping.

(2) The strongest transitions observed are inelastic scattering and single-nucleon transfer reactions. In particular, four transitions, the inelastic excitation of ^{48}Ca(2^+) and ^{48}Ca(3^-), and the single-nucleon transfers ^{48}Ca(^{16}O, ^{15}N)^{49}Ca($\frac{7}{2}^-$)g.s. and ^{48}Ca(^{16}O, ^{17}O)^{47}Ca($\frac{7}{2}^-$)g.s. account for ≈25% of the entire direct reaction strength.[71] The cross sections decrease rapidly as more nucleons are transferred (i.e., factors of 5–10 per nucleon transferred). As the number of protons stripped increases it is observed that the reaction strength shifts from low-lying levels in the residual nucleus to higher excitation energy.

(3) The single and multinucleon transfer reactions show a strong selectivity in the levels populated. In cases where comparison is possible this selectivity appears to be the same as that observed in light-ion induced reactions after the differences in kinematic matching conditions are taken into account.

(4) The shapes of the angular distributions observed show a clear evolution as a function of the number of nucleons transferred. Specifically, for single-nucleon transfers there is prominent strength near the grazing angle which disappears as more nucleons are transferred. For the multinucleon transfers which are well matched a pronounced forward angle diffraction structure is observed which is characteristic of the L transfer. As the reaction becomes more poorly matched, this diffraction structure is rapidly damped resulting in a smoothly varying forward peaked distribution. Such an evolution as function of nucleons transferred and matching conditions is clearly seen when all channels are measured simultaneously as in this study.

(5) Transfer reactions were observed which could only proceed via multistep sequential processes [i.e., (^{16}O, ^{15}C), (^{16}O, ^{17}N), and possibly (^{16}O, ^{16}N)]. These reactions give an indication of the importance of such processes and are observed to be roughly of the same strength as transfers observed for "cluster" transfer involving the same number of nucleons.

From comparison of theoretical calculations with experiment, additional conclusions can be drawn:

(1) *Inelastic scattering.* Comparison of DWBA calculations for inelastic scattering to the ^{48}Ca(2^+) and ^{48}Ca(3^-) states with experiment shows that reasonably good fits can be obtained. However, the detailed behavior is not reproduced and, in particular for the ^{48}Ca(2^+) state, a nuclear deformation different from the charge deformation is needed to reproduce the observed magnitude. Microscopic form factor and coupled-channels calculations would be of interest to investigate these discrepancies.

(2) *Single-nucleon transfers.* DWBA calculations for single-nucleon transfers to single-particle or hole states are found to reproduce the absolute cross section to ≈20% and the observed shapes of the angular distributions fairly well. For the transfers to the more weakly populated states, for example, the 1p-2h state in ^{47}Ca and the [^{17}O*($\frac{1}{2}^+$) ⊗ ^{47}Ca($\frac{7}{2}^-$)g.s.] in the (^{16}O, ^{17}O) reaction, DWBA calculations are unable to reproduce either the strength or the shapes of the angular distributions observed. It is of interest to know whether inclusion of more complex reaction processes would result in a better description of the data.

(3) *Multinucleon transfers.* Comparison of DWBA calculations with the measured angular distributions reveal that similar discrepancies between theory and experiment are found in essentially all cases considered: namely, the strength predicted near the grazing angle is not observed in the data, and the absolute cross sections are too small by factors of 2–1000. The calculated shapes of one-step processes are not appreciably altered by the inclusion of two-step sequential transfer, although much better agreement in the magnitudes is obtained. It therefore becomes of interest to see whether coupled-channels contributions can provide the necessary alterations in both magnitude and shape.

In summary, comparison of conventional DWBA calculations with measured angular distributions for inelastic scattering and transfer reactions ob-

served in the $^{16}O + ^{48}Ca$ reaction at $E_{lab} = 56$ MeV reveals that DWBA theory poorly reproduces experiment for a large fraction of the transitions considered. The possible explanation suggested by the calculations performed for some of the transitions discussed here and those observed in other reactions is that more complex reaction processes play an important role. If such a strong interdependence between the various direct channels exists then experimental information for several reaction channels must be used to fully understand any single channel. In this study we present experimental measurements for all reaction channels of significant strength and thereby sufficient data to provide guidance, as well as a stringent test, for theoretical models which are applied.

ACKNOWLEDGMENTS

The authors wish to express their thanks to the tandem operating staff for their efforts and cooperation. Thanks are also extended to Dr. K.-E. Rehm for participation in taking some of the data presented here. We are indebted to Dr. M. H. Macfarlane and Dr. Steven C. Pieper for making available their reaction code Ptolemy and for extensive discussions of the DWBA calculations. Useful discussions pertaining to this study with Dr. D. Geesaman and Dr. J. P. Schiffer are gratefully acknowledged. The work was performed under the auspices of the USERDA, Division of Physical Research.

---

*Present address: Weizmann Institute of Science, Rehovoth, Israel.
†Present address: University of Pennsylvania, Philadelphia, Pennsylvania 19174.
‡Present address: Australian National University, Canberra, Australia.
§Present address: Technical University of Munich, Munich, West Germany.
**Present address: Indiana University, Bloomington, Indiana 47401.

[1]Useful references on heavy-ion induced inelastic and transfer reactions can be found in the following conference proceedings: (a) Argonne National Laboratory Informal Report Physics No. 1973B, 1973 (unpublished), Vols. I and II; (b) *International Conference on Nuclear Physics*, edited by J. de Boer and H. J. Mang (North-Holland, Amsterdam, 1973), Vol. I and II; (c) *International Conference on Reactions between Complex Nuclei*, edited by R. L. Robinson, F. K. McGowan, J. B. Ball, and J. H. Hamilton (North-Holland, Amsterdam, 1974), Vols. I and II; (d) *Symposium on Classical and Quantum Mechanical Aspects of Heavy Ion Collisions*, Lecture Notes in Physics, edited by H. L. Harney, P. Braun-Munzinger, and C. K. Gelbke (Springer, Berlin, 1975).

[2]See for example, Argonne National Laboratory, Informal Report Physics No. ANL/PHY-76-2, 1976 (unpublished), Vols. I and II.

[3]See for example, M. Lefort, Y. Le Beyec, and J. Pe'ter, in *Proceedings of the International Conference on Reactions between Complex Nuclei*, edited by R. L. Robinson, F. K. McGowan, J. B. Ball, and J. H. Hamilton (North-Holland, Amsterdam, 1974), Vol. I, p. 81; M. Lefort J. Phys. (Paris), Colloque C5, Suppl.-II, 37, C5-57 (1976).

[4]D. Glas and U. Mosel, Phys. Rev. C 10, 2620 (1974).

[5]R. Bass, Nucl. Phys. A231, 45 (1974).

[6]B. Zeidman, W. Henning, and D. G. Kovar, Nucl. Instrum. Methods 118, 361 (1974).

[7]E. J. Williams, Proc. R. Soc. A135, 109 (1934).

[8]J. R. Erskine, T. H. Braid, and J. C. Stoltzfus, Nucl. Instrum. Methods 135, 67 (1976).

[9]F. G. Perey, optical-model code GENOA (unpublished).

[10]E. H. Auerbach, Brookhaven National Laboratory Report No. BNL 6532, 1962 (unpublished); modified by S. A. Zawadski, Argonne National Laboratory.

[11]W. Henning, Y. Eisen, J. R. Erskine, D. G. Kovar, and B. Zeidman, Phys. Rev. C 15, 292 (1977).

[12]E. Rehm, J. R. Erskine, W. Henning, and D. G. Kovar, Bull. Am. Phys. Soc. 22, 565 (1977); (unpublished).

[13]D. H. Gloeckner, M. H. Macfarlane, and S. C. Pieper, Argonne National Laboratory Report No. ANL-76-11 (1976) (unpublished).

[14]R. H. Bassel, G. R. Satchler, R. M. Drisko, and E. Rost, Phys. Rev. 128, 2693 (1962).

[15]A. Winther and J. de Boer, in *Coulomb Excitation*, edited by K. Alder and A. Winther (Academic, New York, 1966), p. 103.

[16]R. A. Eisenstein, D. W. Madsen, H. Theisson, L. S. Cardman, and C. K. Bockelman, Phys. Rev. 188, 1815 (1969).

[17]N. Benczer-Koller, G. G. Seaman, M. C. Bertini, J. W. Tape, and Jaul R. MacDonald, Phys. Rev. C 2, 1037 (1970).

[18]F. D Becchetti, D. G. Kovar, B. G. Harvey, J. Mahoney, B. Mayer, and F. G. Puhlhofer, Phys. Rev. C 6, 2215 (1972).

[19]P. R. Christensen, I. Cheenov, E. E. Gross, R. Stokstad, and F. Videbaek, Nucl. Phys. A207, 433 (1973).

[20]J. L. Ford, K. S. Toth, D. C. Hensley, R. M. Gaedke, P. J. Riley, and S. T. Thornton, Phys. Rev. C 8, 1912 (1973).

[21]E. E. Gross, H. G. Bingham, M. L. Halbert, D. C. Hensley, and M. J. Saltmarsh, Phys. Rev. C 10, 45 (1974).

[22]K. E. Rehm, H. J. Körner, M. Richter, H. P. Rother, J. P. Schiffer, and H. Spieler, Phys. Rev. C 12, 1945 (1975).

[23]C. R. Gruhn, T. Y. T. Kuo, C. J. Maggiore, and B. M. Preedom, Phys. Rev. C 6, 944 (1972).

[24]A. Tellez, R. Ballini, J. Delaunay, and J. P. Fouan, Nucl. Phys. A127, 438 (1969).

[25]F. T. Baker, S. Davis, C. Glashausser, and A. B. Robbins, Nucl. Phys. A250, 79 (1975).

[26]E. P. Lippincott, and A. M. Bernstein, Phys. Rev.

163, 1170 (1967).
[27]K. S. Low, Phys. (Paris), 37, C5-15 (1976); D. L. Hillis, E. E. Gross, D. C. Hensley, L. D. Rickertsen, C. R. Bingham, A. Scott, and F. T. Baker, Phys. Rev. Lett. 36, 304 (1976).
[28]W. Henning, D. G. Kovar, B. Zeidman, and J. R. Erskine, Phys. Rev. Lett. 32, 1015 (1974).
[29]W. Henning, D. G. Kovar, J. R. Erskine, and L. R. Greenwood, Phys. Lett. 55B, 49 (1975).
[30]J. R. Erskine, A. Marinov, and J. P. Schiffer, Phys. Rev. 142, 633 (1966).
[31]G. Bruge, H. Faraggi, Ha Duc Long, and P. Roussel, Saclay Report No. CEA-N-1232, 124, 1970 (unpublished).
[32]D. D. Armstrong, and A. G. Blair, Phys. Lett. 10, 204 (1964); Phys. Rev. 140, B1226 (1965).
[33]M. S. Zisman, F. D. Becchetti, B. G. Harvey, D. G. Kovar, J. Mahoney, and J. D. Sherman, Phys. Rev. C 8. 1866 (1973).
[34]R. M. DeVries, G. R. Satchler, and J. G. Cramer, Phys. Rev. Lett. 32, 1377 (1974).
[35]J. C. Hiebert, E. Newman, and R. H. Bassel, Phys. Rev. 154, 898 (1967).
[36]H. Doubre, D. Royer, M. Aediti, L. Bimbot, N. Frascaria, J. P. Garron, and M. Riou, Phys. Lett. 29B, 355 (1969).
[37]W. J. Pinkston and G. R. Satchler, Nucl. Phys. 72, 641 (1965).
[38]P. Martin, M. Buenerd, Y. Dupont, and M. Chabre, Nucl. Phys. A185, 564 (1973).
[39]F. Ajzenberg-Selove, Nucl. Phys. A166, 1 (1971).
[40]M. D. Cooper, W. F. Hornyak, and P. G. Roos, Nucl. Phys. A218, 465 (1972).
[41]R. J. Peterson, Phys. Rev. 170, 1003 (1969).
[42]J. L. Yntema, Phys. Rev. 186, 1144 (1969).
[43]D. Schmitt, and R. Santo, Z. Phys. 233, 114 (1970).
[44]K. Pruess, G. Delic, L. A. Charlton, and N. K. Glendenning, in Proceedings of the Symposium on Macroscopic Features of Heavy-Ion Collisions [ANL Report No. ANL/PHY-76-2 (unpublished)], Vol. 2.
[45]G. Delic, K. Pruess, L. A. Charlton, and N. K. Glendenning, Report No. LBL 5074 (unpublished).
[46]N. K. Glendenning, in *Proceedings of the International Conference on Reactions between Complex Nuclei* (see Ref. 1), Vol. 2, p. 137.
[47]R. J. Ascuitto, and J. S. Vaagen, in *Proceedings of the International Conference on Reactions Between Complex Nuclei* (see Ref. 1), Vol. 2, p. 257.
[48]G. Sherwood, Bull. Am. Phys. Soc. 21, 65 (1976).
[49]D. Evers, W. Assman, K. Rudolph, S. J. Skorka, and P. Sperr, Nucl. Phys. A230, 109 (1974).
[50]Y. Eisen, H. T. Fortune, W. Henning, D. G. Kovar, S. Vigdor, and B. Zeidman, Phys. Rev. C 13, 699 (1976).
[51]W. Schlegel, D. Schmitt, R. Santo, and F. Pühlhofer, Nucl. Phys. A153, 502 (1970).
[52]H. Ohnuma, J. R. Erskine, J. A. Nolen, J. P. Schiffer, and P. G. Roos, Phys. Rev. 177, 1695 (1969).
[53]C. Moazed, K. Nagatani, and A. M. Bernstein, Nucl. Phys. A139, 1 (1969).
[54]H. Hefele, U. Lynen, and R. Santo, Nucl. Phys. A157, 93 (1970).
[55]R. Middleton and D. J. Pullen, Nucl. Phys. 51, 63 (1964).
[56]I. Talmi, Helv. Phys. Acta. 25, 185 (1952); M. Moshinsky, Nucl. Phys. 13, 104 (1959).
[57]N. K. Glendenning, Phys. Rev. 137, B102 (1965).
[58]H. J. Korner, G. C. Morrison, L. R. Greenwood, and R. H. Siemssen, Phys. Rev. C 7, 107 (1973).
[59]J. D. Garrett, in *Classical and Quantum Mechanical Aspects of Heavy-Ion Collisions*, edited by H. L. Harney, P. Braun-Munzinger, and C. K. Gelbke (Springer, Heidelberg, 1975), p. 59, and references therein.
[60]D. H. Feng, T. Udagawa, and T. Tamura, Nucl. Phys. A274, 252 (1976).
[61]T. Kammuri, Nucl. Phys. A259, 343 (1976).
[62]B. F. Bayman, Phys. Rev. Lett. 32, 71 (1974).
[63]P. D. Bond, C. Chasman, J. D. Garrett, C. K. Gelbke, Ole Hansen, M. J. LeVine, A. Z. Schwarzchild, C. E. Thorn, Phys. Rev. Lett. 36, 300 (1976).
[64]K. S. Low, T. Tamura, and T. Udagawa, Phys. Lett. 67B, 5 (1977).
[65]S. Kubono, D. Dehnhard, D. A. Lewis, T. K. L., J. L. Artz, D. J. Weber, P. J. Ellis, and Dudek-Ellis, Phys. Rev. Lett. 38, 817 (1977).
[66]H. T. Fortune, W. Henning, D. G. Kovar, B. Zeidman, and Y. Eisen, Phys. Lett. 57B, 445 (1975).
[67]A. Richter, J. R. Comfort, N. Anantaraman, and J. P. Schiffer, Phys. Rev. C 5, 821 (1972).
[68]C. Garrde, T. Kammuri, and F. Osterfeld, Nucl. Phys. A222, 579 (1974).
[69]D. G. Kovar, W. Henning, B. Zeidman, Y. Eisen, and H. T. Fortune, Phys. Rev. Lett. 33, 1611 (1974).
[70]T. Udagawa, T. Tamura, and K. S. Low, Phys. Rev. Lett. 34, 30 (1975).
[71]D. G. Kovar, W. Henning, B. Zeidman, Y. Eisen, H. T. Fortune, and S. E. Vigdor, (unpublished).